 doi:10.20944/preprints201801.0123.v1

Type of the Paper (Article)

Three-Dimensional Facies Analysis using Object-Based Geobody Modeling: A Case Study for the Farewell Formation, Maui Gas Field, Taranaki Basin, New Zealand

AKM Eahsanul Haque[1]*, Md. Aminul Islam[1] and Mohamed Ragab Shalaby[1]

[1] Department of Physical and Geological Sciences, FoS, Universiti Brunei Darussalam, Jalan Tungku Link, Gadong BE-1410, Brunei Darussalam; aminul.islam@ubd.edu.bn

* Correspondence: akmeahsan@yahoo.com; Tel.: +673-7219745

Abstract: The early-mid Paleocene Farewell Formation is stratigraphically distributed across the southern Taranaki Basin (STB) which is also encountered within the Maui Gas Field. Using available 3D seismic and well log data, a challenging task to delineate the spatial distribution and geobody patterns of the potential reservoir sands of the formation was performed. Object based modeling coupled with sequential indicator simulation were used to analyze the spatial distribution of facies configuration and a conceptual model was developed based on the outputs from the structurally- modeled grids. The facies modeling followed a hierarchical object-based mechanism which was set to perform with constraints like channel geometry and heterogeneity within the formation. The resultant 3D geobody model showed that the distributary channels, mainly braided geobodies flowed from northeast cutting through several regional normal-fault systems to the southwest. Overbank facies was adhered to the fringe of the channels whereas the floodplain facies was at the periphery of the model. Meandering channel-sand facies were mostly observed at the center of the model flowing in a more random manner, occupying major flow directions of northwest to southwest and southeast to northwest within the model.

Keywords: Geobody Modeling, Object-Based Facies Modeling (OBFM), Variogram Analysis, Farewell Formation, Paleo-depositional Environment.

1. Introduction

The Maui Field produces gas from three main reservoirs of Paleocene to Eocene in age. Farewell Formation is the deepest and the thinnest of the reservoirs of this gas field having measured drilling depths ranging from 3100-3200m TVDSS [1-4]. The Farewell Formation in the Maui Gas Field includes gas and condensate-saturated interval of approximately 100m thickness. The reservoir interval consists of highly discontinuous fluvial sandstones and associated siltstones and shales deposits as identified in the well log responses. The main reservoir sandstones are braided and meandering stacked channel sand deposits that are highly lenticular, with lateral dimensions ranging from few hundred to several kilometres in length [5-8]. Crevasse-splay deposits comprise a relatively lower proportion of the overall sandstone volume and are generally of lower reservoir quality [5].

Therefore, an understanding of the structure as well as the thickness, distribution and connectivity of the sandstone deposits as separate geobody units are important for the well planning during future development of the field. This is significant because during well planning phase, 500-1500m spacing between wells is often necessary to effectively deplete the reservoir given the limited lateral extent of the fluvial sandstones within prospective formations like that of Farewell [9-10]. Even with intensive development of the Farewell reservoir with spacing of 1-2 km for future

Preprints (www.preprints.org) | NOT PEER-REVIEWED | Posted: 15 January 2018 doi:10.20944/preprints201801.0123.v1

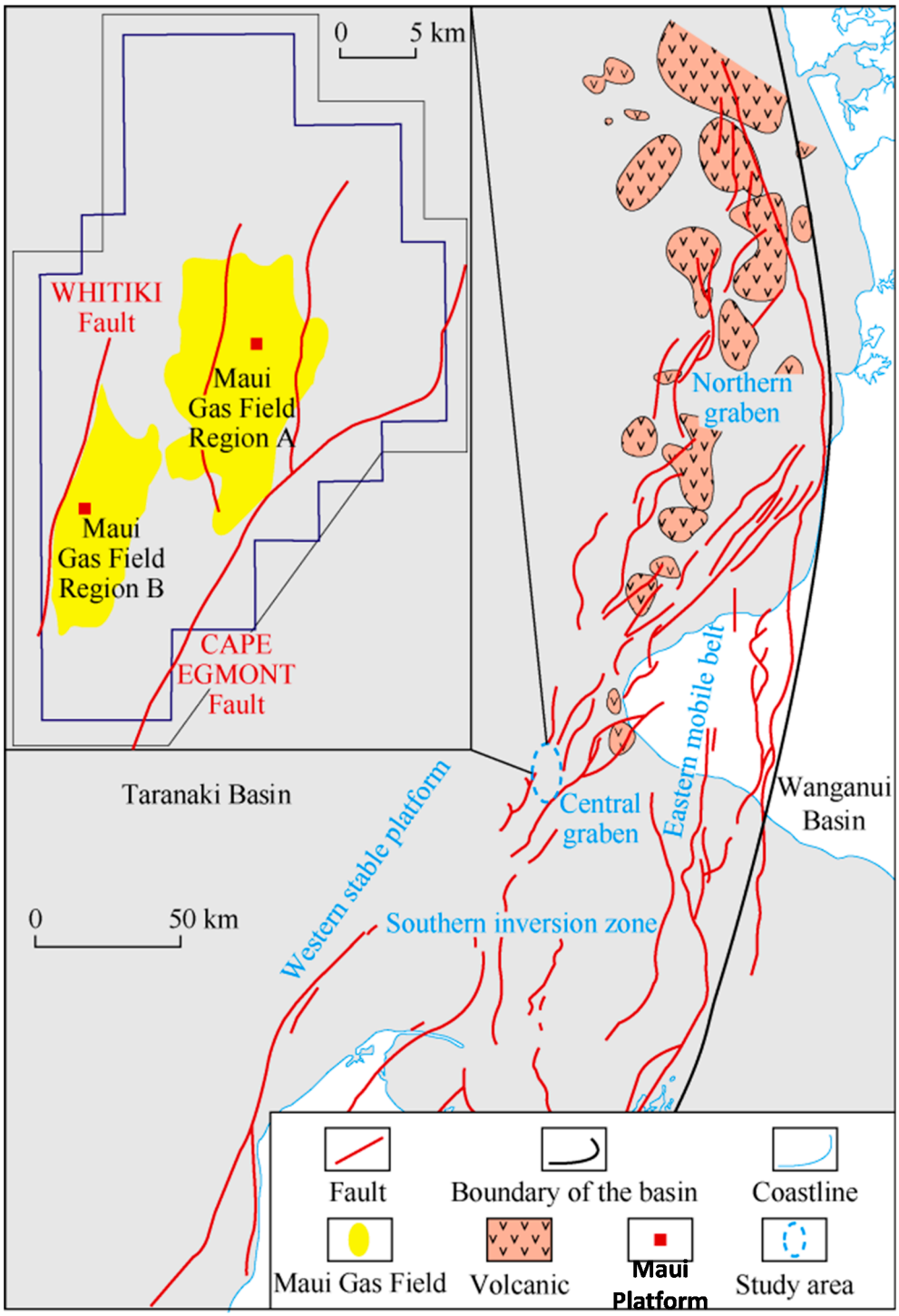

Figure.1. Maui Gas Field and the surrounding regions of the Taranaki Basin, New Zealand (after Haque et al. 2016). The yellow colored compartments are two producing blocks of the Maui Gas Field. N-S elongated lines are the major faults cutting through the gas field. The gas field sits on the Central Graben which is located at the Southern Taranaki Basin (STB).

drillings, bottom-hole pressure tests revealed that almost all the major sand packages tested in all four wells were in pressure communication showing partial pressure depletion [11-13].

The primary objectives of this study were (1) to interpret the primary stratigraphic framework of the Farewell interval within the study area of the Maui Gas Field, (2) to characterize and model lithology distribution according to the environment of deposition, (3) to explain the predicted fluvial sand-bodies within the reservoir and paleo-depositional modeling of the Farewell reservoir for deeper reservoir predictions.

Preprints (www.preprints.org) | NOT PEER-REVIEWED | Posted: 15 January 2018 doi:10.20944/preprints201801.0123.v1

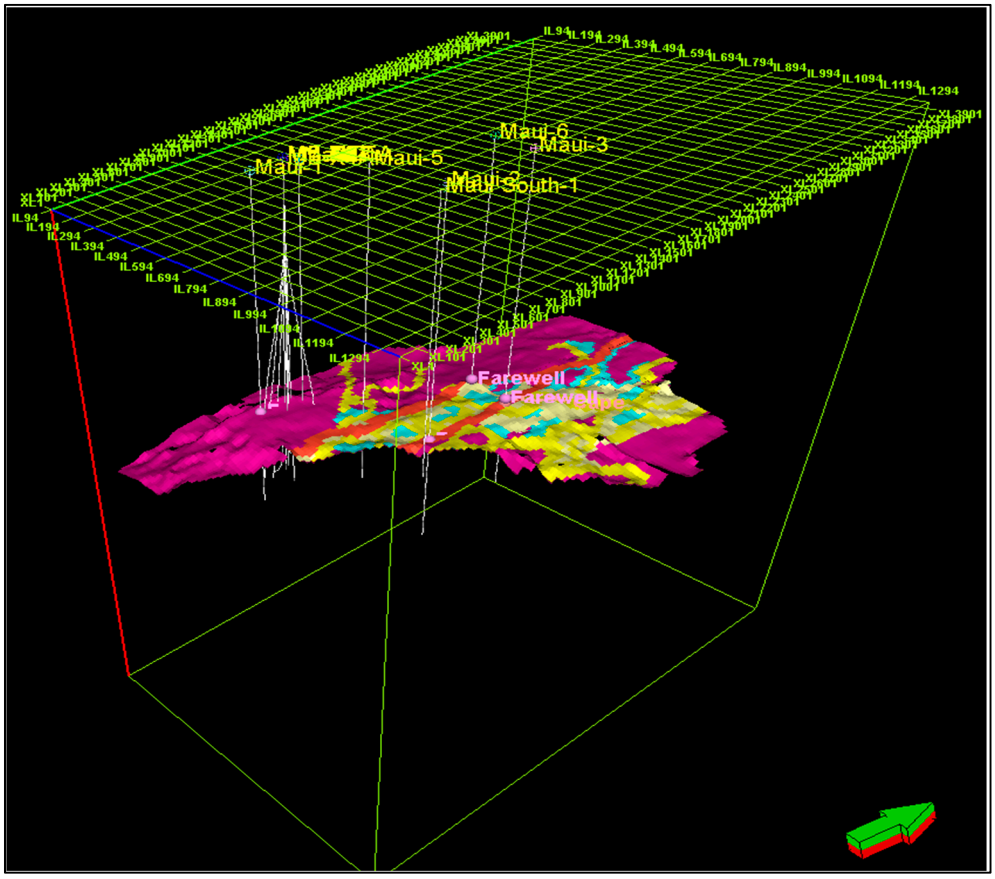

Figure.2. Seismic cube of the Maui Gas Field showing well locations and 3D geomodel of the Farewell Formation.

The study area is within the northern portion of the offshore Taranaki Basin (Fig.1) and includes well information and 3D seismic data. The seismic survey covers an area of ~150 sq. km with average grid size of the cube being 50m X 50m (Fig.2). The interval of interest for this study approximately coincides with the mainly condensate/gas-productive interval at the Maui Gas Field and includes an average of ~100m thick interval of the Farewell Formation.

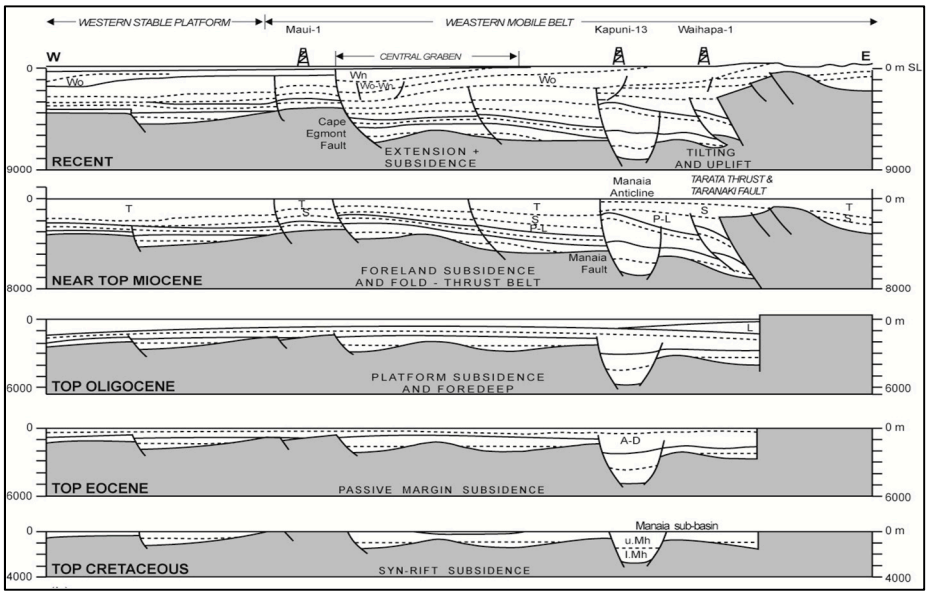

Figure.3. Regional Structural setup of the Taranaki Basin. Grey shading represents basement (after King and Thrasher 1996). The pre-Miocene configuration of the basin's eastern margin is uncertain (Reilly et al. 2015). Depth scale in metres below sea level. Vertical exaggeration = 5. The restorations are based on present-day

Preprints (www.preprints.org) | NOT PEER-REVIEWED | Posted: 15 January 2018 doi:10.20944/preprints201801.0123.v1

sediment thicknesses, and incorporate paleo-bathymetry; no allowance was made for sediment de-compaction, and the sections have not been structurally balanced. The original thickness of Miocene sediment is uncertain.

2. Geological Setup and Stratigraphy

The Taranaki Basin has a composite morphology resulting from diverse episodes of tectonic activity [2, 14-15]. It consists of several superimposed sub-basins, depocentres, and areas of uplift, that range in age from mid-Cretaceous to Recent (Fig.3). The basin's structural development was influenced by contrasting Australian-Pacific plate boundary kinematics in the Late Cretaceous-Paleocene and in the Oligocene-Neogene, separated by a relatively quiescent period throughout most of the Eocene [6, 16-18]. Taranaki Basin is broadly divided into Western Stable Platform and the Eastern Mobile Belt [6-7, 18], and Maui Gas Field sits on the EMB. EMB in the previous literatures reflects the composite architecture and evolution of the basin, involving several tectonic phases of differ in age, origin and style [8, 19-20].

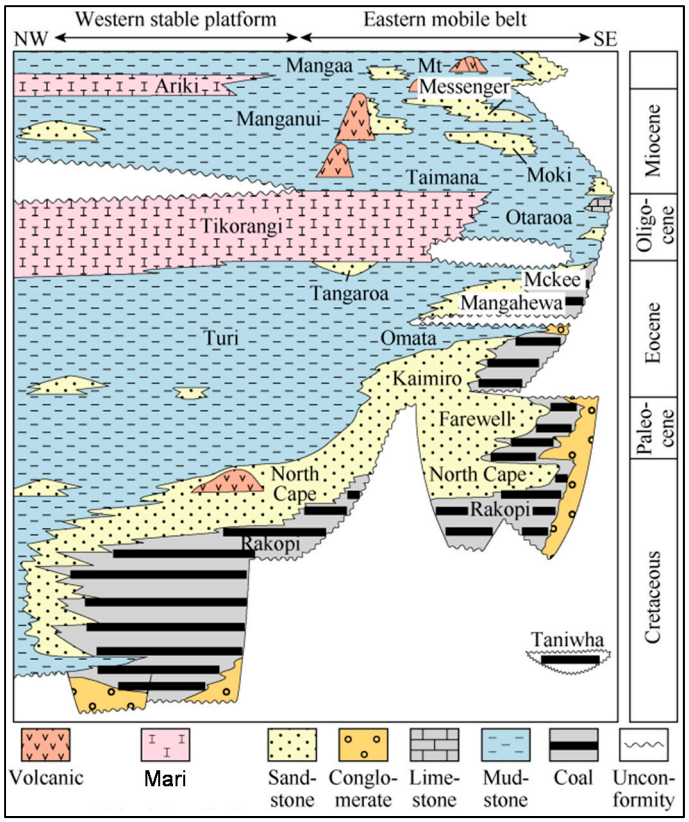

Figure.4. Generalized Stratigraphy of the Taranaki Basin. Farewell Formation is at the bottom of the Paleocene period of the Taranaki stratigraphy (after King and Thrasher 1996). Parts of the yellow colored (dotted) sands are Farewell Formation on the stratigraphic chart.

Stratigraphically Farewell Formation falls within Kapuni Group of Paleocene age (Fig.4). Paleocene and Eocene deposits belong to the laterally equivalent Kapuni and Moa groups, which constitute a late-rift and post-rift transgressive sequence [6, 18]. The Apart from Farewell Formation, Kapuni Group also consists of Kaimiro, Mangahewa, and McKee formations. It is predominantly terrestrial, including some marginal marine deposits [6-8]. A paraconformity at the top of the Moa-Kapuni succession reflects waning subsidence and sediment supply, and marks the culmination of this depositional phase in the latest Eocene-Early Oligocene.

Preprints (www.preprints.org) | NOT PEER-REVIEWED | Posted: 15 January 2018 doi:10.20944/preprints201801.0123.v1

3. Materials and Methods

3.1. Dataset

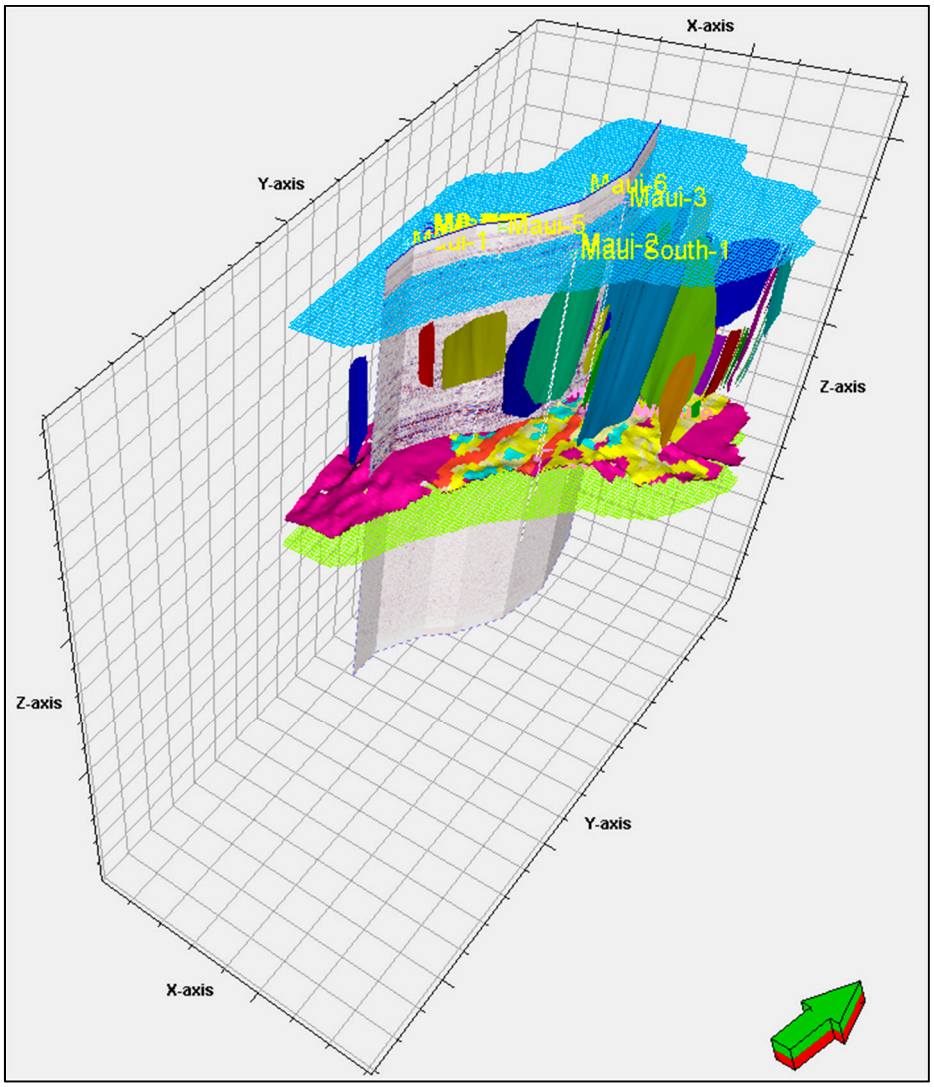

Figure.5. The Farewell model is identified in accordance with the 3D seismic interpretation from the Maui cube. The mesh grill top and bottom (blue and yellow) are model boundaries whereas the different coloured vertical pillars are the faults interpreted along the entire 3D structural grid of the Maui Gas Field. The seismic surface (pink coloured) denotes the interpreted Farewell reservoir zone.

The first well of the Maui Gas Field has been drilled in 1969 and the last so far being drilled in early 2000s; we have used 17 available well data for the current study from which 4 wells have encountered Farewell Formation. In order to move forward for greater accuracy in delineating possible geobodies, we utilized well location data along with the log data. A detailed collection of conventional well log have been available for the study, namely Gamma Ray (GR), Caliper, Resistivity (Shallow/Deep), Neutron, Density and Sonic. A set of formation tops of the Farewell Formation for all the available wells were also utilized. 3D seismic data on the Maui Gas Field was the basis for the study on which the model was built and studied. Velocity model was later generated for the conversion of the seismic cube from time to depth domain. Farewell horizon was identified based on the formation top, seismic signature and regional geological understanding. For the Farewell Formation, there were no available core data and therefore the 3D depositional facies reconstruction was largely dependent on well log interpretation and seismic attribute analysis of the Farewell Formation.

Preprints (www.preprints.org) | NOT PEER-REVIEWED | Posted: 15 January 2018 doi:10.20944/preprints201801.0123.v1

3.2. Three-Dimensional Structural Reconstruction

Structural reconstruction was the key component for this study because it acted as the primary skeletal for the geobodies modeling. A grid resolution of 50X50m was used for our

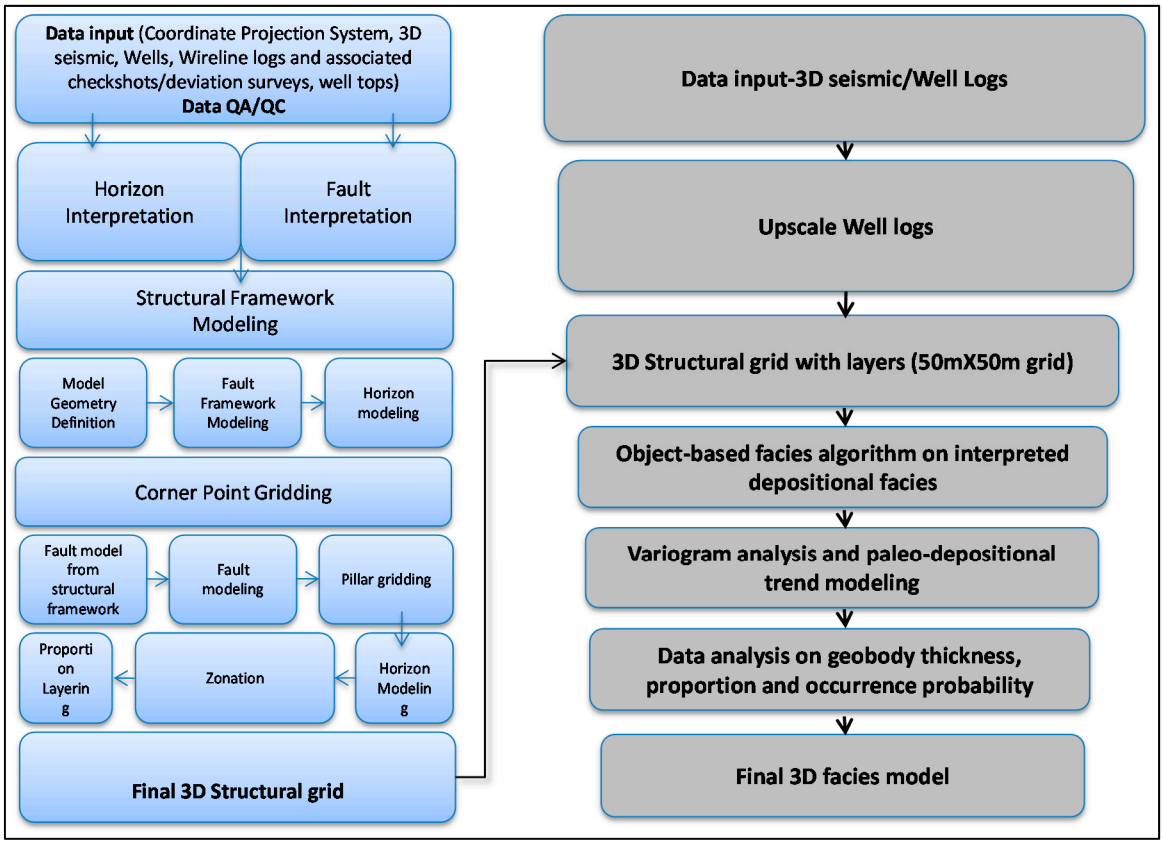

Figure.6. Standardized workflow for the 3D facies modeling of the Farewell Formation, Maui Gas Field, Taranaki Basin. The entire workflow is divided into two segments; first being the construction of the 3D geo-grid of the gas field (left) followed by the objected-based process for building the facies model of the Farewell Formation.

study. The grid resolution was solely based on the average thickness of the Farewell reservoir and the spatial dimension within the Maui Gas Field. Volume Based Modeling (VBM) was used in reconstruction of the structural model. Schlumberger's Petrel 2013.1 software was used to model the studied formation. The volume-based structural model proposed earlier [21] was used as a skeleton for our study.

Initially the farewell zone was identified within the seismic cube (in depth) along with possible faults that had cut through the zone and the horizon-fault system was incorporated within horizon modeling phase (Fig.5). This incorporation ultimately placed the zone boundary of the Farewell and ensured the connectivity of the faults and their seals for the reservoir [21].

During the next phase, structural gridding was performed using stair-stepping of the fault frameworks within the model and then subsequent pillar gridding along the Fault Framework Model (FFM). It was observed that according to the structural model, the regional dip of the Farewell Formation was around 12° in the north and 17° in the south. Most of the faults that cut through Farewell Formation were of extensional in nature [2, 21] and strikes NE-SW with an average dip angle of 60-70° [21].

3.3. Workflow

Object-Based Facies Modeling (OBFM) allowed us to populate discrete logical facies model with specific objects (geobodies such as paleo-channels etc.) which were generated and distributed stochastically [22-26]. This study was completely based on geometrical inputs that control particular body shapes (thickness/width etc.). It was important to note that OBFM built for the study was

Preprints (www.preprints.org) | NOT PEER-REVIEWED | Posted: 15 January 2018 doi:10.20944/preprints201801.0123.v1

constrained by the well log which honours the well log as well as insertion of the facies as "bodies" within the model. We also used proper erosional/replacement rules for different "geobodies" based on their spatial distribution in space. Vertical and areal trends were used for defining the spatial distribution [22, 27-31].

Facies modeling workflow for the Farewell Formation followed three robust steps based on the above mentioned strategies. During the initial stage, (1) depositional-bodies were generated using stochastic algorithm. (2) defining the boundaries of the interpreted geobodies, (3) finally the internal geometry and heterogeneity of the facies were developed to generate the final OBFM of the Farewell Formation (Fig.6).

In this study, we used 3D objects like paleo-channels and simulated the channels with levees in the model. For defining the shape of the objects, 3D-pipe and ellipsoid shapes were selected to create the geobodies within the OBFM process [27, 30].

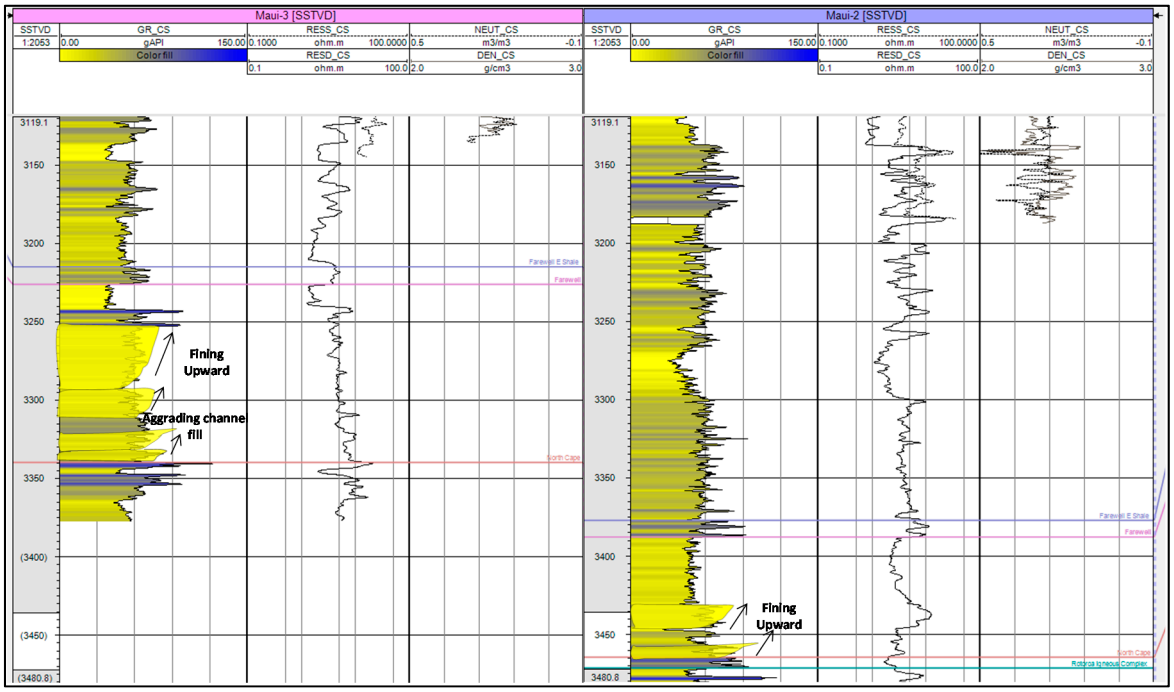

Figure.7. Meandering channel sand deposits in Maui-3 and Maui-2 wells. Log response clearly shows multiple fining-upwards cycles as interpreted on the GR logs of both the wells. Stacked sand bodies are evident from the log interpretation. Aggrading channel-fills are also seen in Maui-3 well.

3. Results

Three (3) depositional facies were identified and interpreted within the Farewell Formation. It is to be noted that, there were no physical samples or core cuttings available for this study, therefore the conventional approaches of core-litholog-texture analysis were not followed for this study. Therefore, well log response along with object-based simulation were utilized to interpret all the possible lithologies and subsequent geobodies.

3.1. Meandering Channel Sand Association (Single-Stacked Association)

This facies association was made up of several, 15 to 20 m thick sandstone bodies, that showed sheet geometry in cross-section (width/thickness ratio>30). The basal bounding surfaces of sandstone bodies were flat to concave-up as seen in the well log response of the Maui wells (Fig.7). These basal lags were overlain by different facies, making up distinct facies successions that could be arranged into two main types. The first type was comprised of fine- to medium-grained sandstones, massive or with horizontal cross-bedding [32-35]. The second type was composed of very-fine to medium-grained sandstones containing possible planar and trough cross bedding (~0.5 m thick sets) and could probably be commonly formed ripple cross-lamination [33-34]. Both types showed abrupt

Preprints (www.preprints.org) | NOT PEER-REVIEWED | Posted: 15 January 2018 doi:10.20944/preprints201801.0123.v1

facies shifts and could either form fining-upward cycles or be consistent in grain-size as shown in the log response of Maui-3, Maui-2 and Maui-1 wells.

3.1.1. Interpretation

This facies association was interpreted as fluvial channel deposits. The basal erosion surfaces, overlain by intraformational conglomerates, was associated to 5th order surfaces [36-44]. They represent basal channel boundaries. The sandstone bodies composed of massive and parallel to low-angle cross-bedded sandstones, were interpreted to represent poorly confined sheet flood deposits [41-42]. The common occurrence of both parallel-bedding (upper flow regime) and massive sandstone (hyper-concentrated flows) indicated fast and intermittent, high capacity streams. These channel deposits probably represented fields or trains of individual bedforms that accumulated predominantly by vertical aggradation. This type of architecture was similar to sand-carrying rivers developed on distal braidplains, mostly in arid regions where ephemeral streams normally form a network of shallow channels (distal, sheet flood, sand-bed rivers as explained before [41]. Ancient examples of this fluvial style were studied earlier as well [45-48]. Intraformational conglomerates at the base of the fluvial sandstone packages represented reworking of overbank deposits as interpreted in the log response (Fig.7).

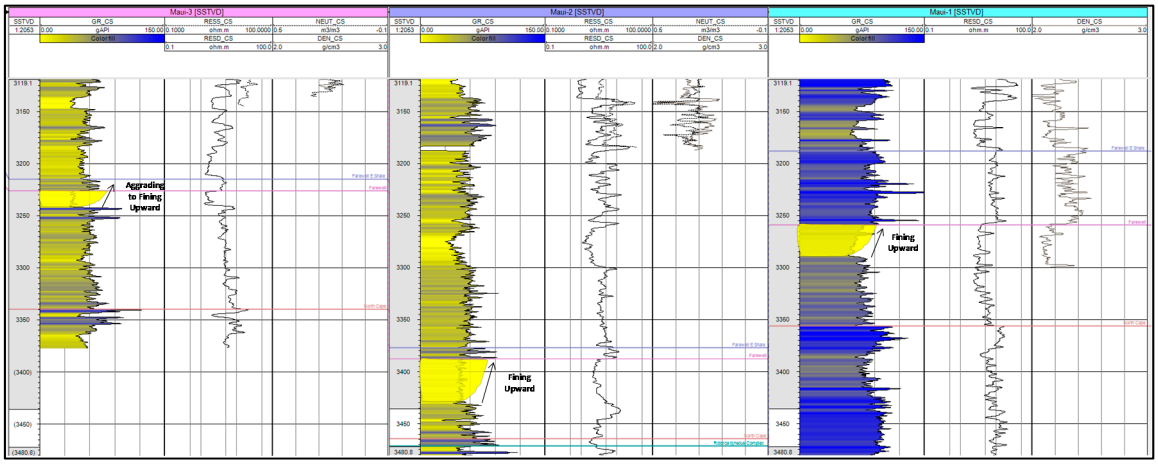

Figure.8. Braided channel sand deposits in Maui-3, Maui-2 and Maui-1 wells. Log response clearly shows fining-upwards cycle at the top of the formation in each well as interpreted on the GR logs. Braided channel sand is thickest in Maui-2 well and thins Northeast towards Maui-3 well.

3.2. Braided Fluvial Channel Belt Facies Association

This facies association was composed of sheet-like sandstone bodies, 20 to 40 m thick. The sandstone bodies were bounded by a flat to concave-up erosional surface and showed internally an upward-fining in grain-size (Fig.8). Locally, fine-grained sandstone, possible massive cross-lamination, occured at the top of units. These relatively large-scale cycles comprised several smaller-scale (5-10 m thick, mean thickness of 7.5 m), fining-upwards sub-cycles (Fig.8).

3.2.1. Interpretation

The fining-upward sandstone bodies bounded by upward concave erosional surfaces (5th order bounding surfaces) [40-41] was interpreted as fluvial channel deposits. Low-angle, down-current dipping surfaces suggested the presence of large-scale, down-current accreting macroforms [41]. The sheet geometry of the sand bodies (width / thickness>30), the prevailing coarse-grained nature of the deposits and the dominance of mid channel bar deposits suggested that this facies association consist of braided fluvial channel belt deposits (Fig.9).

However, it is worth discussing the meaning of the word “channel” within the context of braided rivers for this study. At low discharge, braided rivers form a network of interconnected channels separated by sandy or gravelly bars [44]. To avoid confusion, most authors adopted the term channel-belt to designate the entire river, which was internally subdivided into bars and

Preprints (www.preprints.org) | NOT PEER-REVIEWED | Posted: 15 January 2018 doi:10.20944/preprints201801.0123.v1

enclosing channels [44, 49-51], therefore we also used channel-belt for defining the entire braided system. Herein, sandstone bodies bounded by erosional 5th order bounding surfaces (Miall 1988, 1996) were interpreted as braided channel belts, and were filled with bar and channel floor deposits packages of which were bounded by 4th order surfaces [39-41]. Smaller fining-upward cycles represented the lateral and vertical juxtaposition of bars and channels within the channel-belt [51-55].

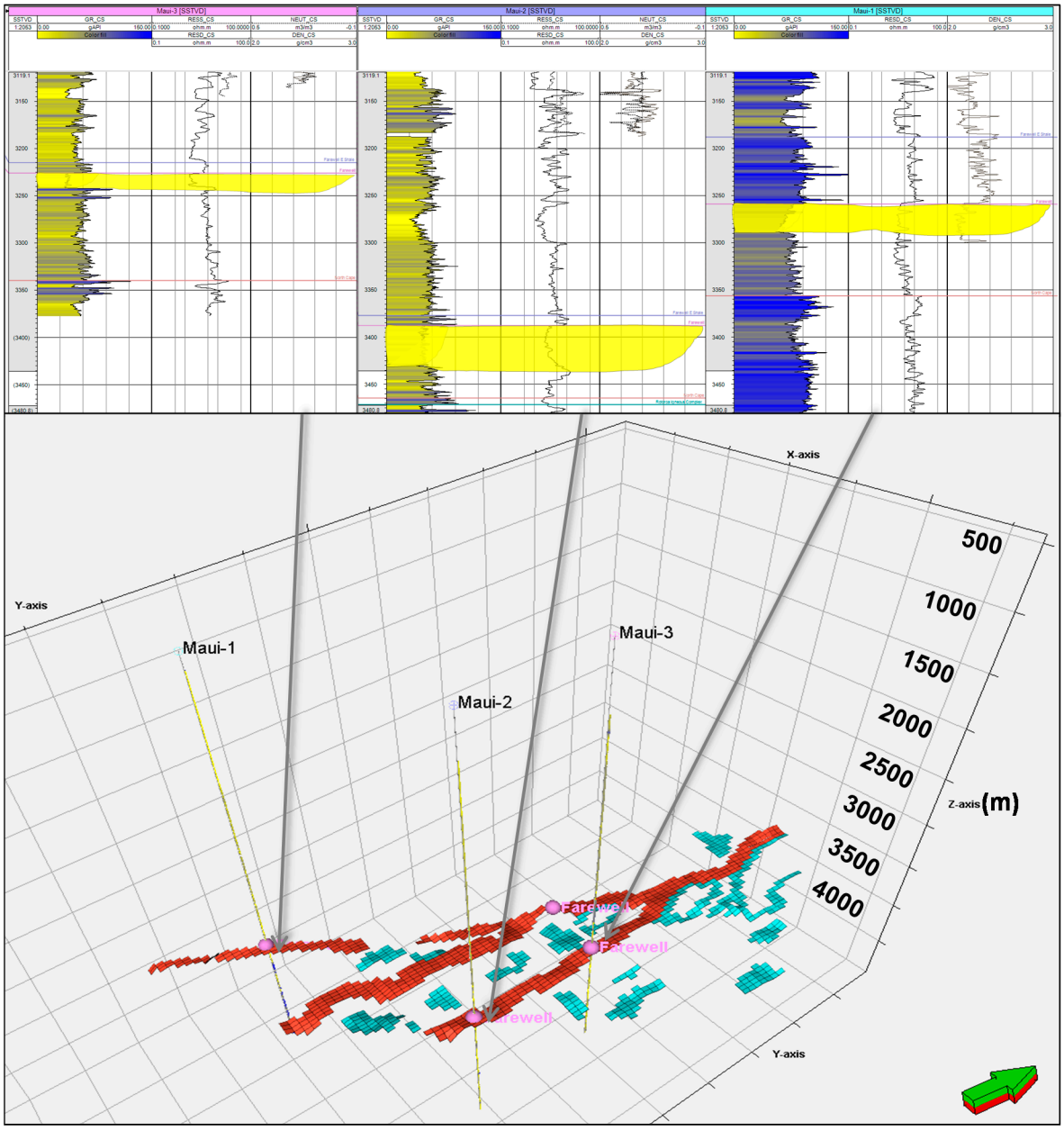

Figure.9. Braided sand bodies as interpreted in the well log responses of the Maui wells. Channel sands are developed from Northeast and have flowed towards Southwest within the Maui Gas Field (top). Note the extensions of the braided channels (Maui-3 and Maui-2) and a distributary from the main braided channel towards Southwest as seen in Maui-1 well (bottom). Red color indicates braided channel sands whereas light blue indicating crevasse splay sands.

3.3. Floodplain Facies Association

This facies association consisted of 2 to 6 m thick, fine- to medium-grained, well-sorted (according to GR response) sandstone units, which was possibly massive in nature. Some sandstone bodies were overlain by massive or laminated mudstone, forming fining-upwards successions (Fig.10). These sandstones were commonly associated with aeolian sand sheet deposits, and their identification was restricted to the subsurface [40-41, 49-51,54].

Preprints (www.preprints.org) | NOT PEER-REVIEWED | Posted: 15 January 2018 doi:10.20944/preprints201801.0123.v1

3.3.1. Interpretation

The aforementioned sedimentary features suggested a link between this facies association and ephemeral shallow streams [23, 41, 56]. Fining-upwards cycles represented complete waning of

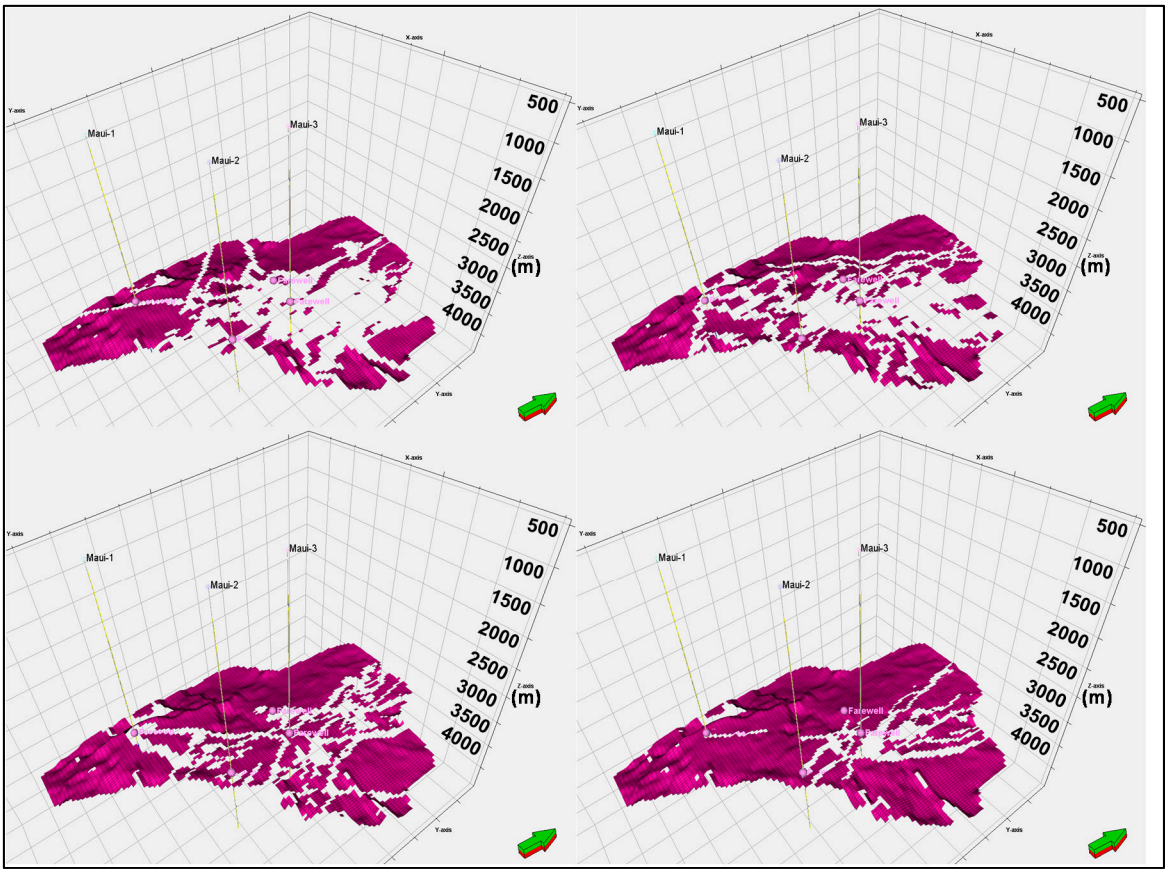

Figure.10. Floodplain deposits are spatially distributed in the facies model. (a) to (d) are suggestive floodplain deposits in different layers within the Farewell Formation; (a) being the shallowest and (d) being the deepest layer of the Farewell Formation. Please note that the floodplain mudstones also define the extent of the sand deposition within the Maui Gas Field as seen in the figure 10(a) to (d). Figure 10(a) represents layer 110 (3200 TVDSS) whereas figure 10(d) represents layer 120 (3300TVDSS) in the model.

flood events. Horizontally stratified sandstones represented the upper plane-bed stability field, at the transition from subcritical to supercritical flow [41], whereas the massive or fluidized sandstones were associated with denser turbulent flows (hyper-concentrated flows), indicating fast and intermittent, high capacity streams. Trough cross bedded sandstones represented residual deposits of 3D dunes formed on the erosional portions of channels, where flow expansion and consequent formation of lower flow regime bedforms took place [56-57].

3.4. Sequence Stratigraphic Framework of the Farewell Formation

One of the main stratigraphic concerns of the last decades entailed the identification and mapping of genetically related units bounded at their top and base by unconformities [41, 58-60]. Following this trend of analyzing the geological record, a large step forward was reached through the development of the sequence stratigraphic method, which has been most widely applied to coastal and shelf deposits [58-61]. Within these depositional settings, sequence accumulation and preservation were controlled by relative sea-level changes.

The identification of systems tracts within fluvial systems was based on several criteria, including geometry and stacking pattern of fluvial channels, channel to overbank deposit ratios. Often, intervals of multi-storey and multi-lateral, amalgamated, sheet sandstone bodies, with rare over-bank deposits were interpreted to record low rates of accommodation space creation [43, 58, 60,

Preprints (www.preprints.org) | NOT PEER-REVIEWED | Posted: 15 January 2018 doi:10.20944/preprints201801.0123.v1

62-63]. On the other hand, intervals characterized by single-storey, ribbon or sheet fluvial channels

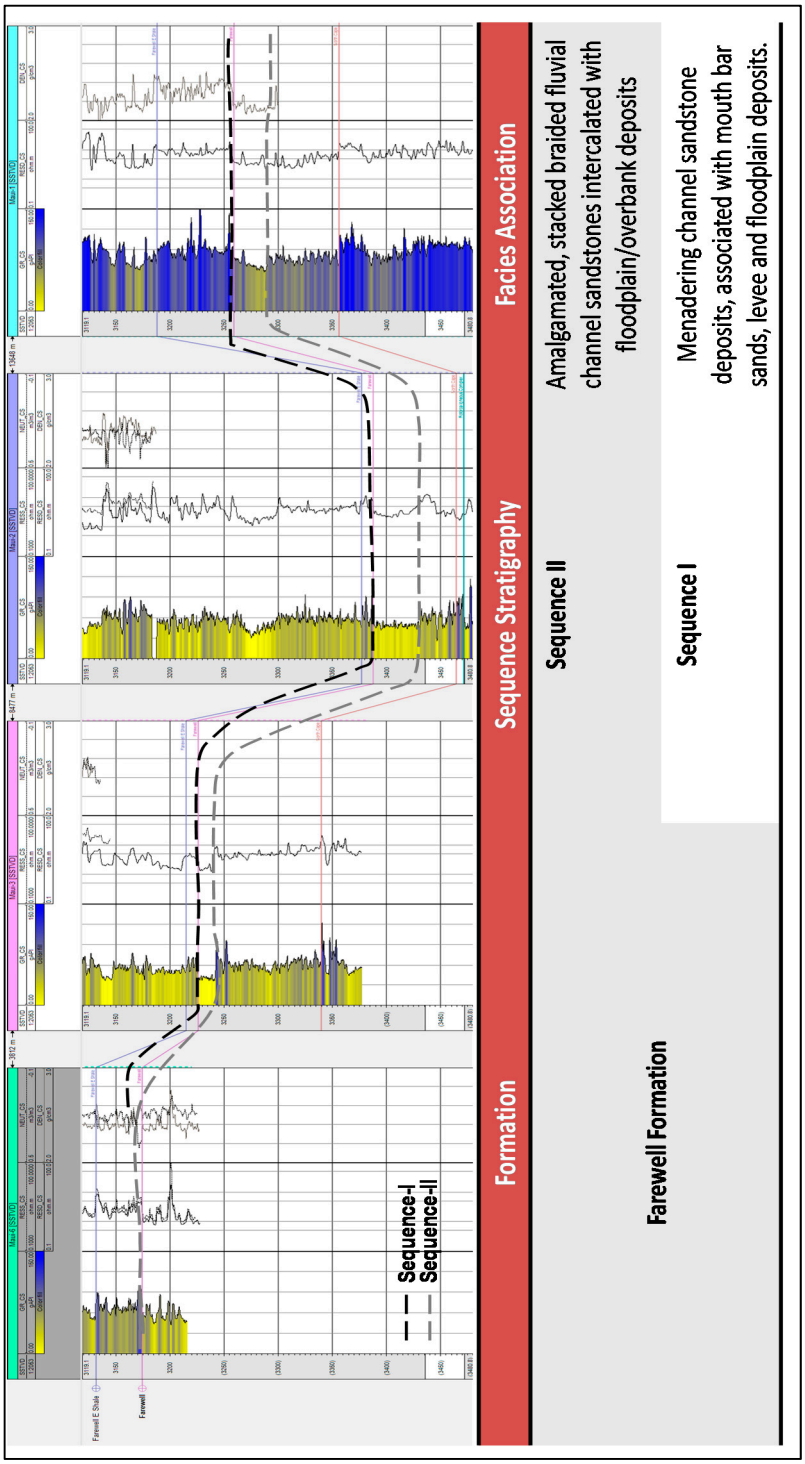

sand bodies encased within fine-grained over-bank deposits were often interpreted to record periods of higher rates of accommodation space creation [43, 63-66].

Figure.11. Sequence Stratigraphy of the Farewell Formation. This formation can be subdivided into two major unconformity based, regional scale depositional sequences as interpreted from the well logs. Sedimentation for the meandering deposits are associated with Sequence I whereas braided channel sands are associated with Sequence II.

The studied interval of the Farewell Formation was herein analyzed using a sequence stratigraphic approach to define depositional sequences, which were defined as "stratigraphic units

Preprints (www.preprints.org) | NOT PEER-REVIEWED | Posted: 15 January 2018 doi:10.20944/preprints201801.0123.v1

composed of a relatively conformable succession of genetically related strata bounded by unconformities or their correlative conformities" [59, 67].

3.4.1. Sequence I

Sequence I was recognized in all studied wells and its minimum thickness ranges from 30-60 m. The lower boundary could not be precisely delineated as it interfingers with the underlying North Cape Formation. Its upper boundary consisted of a regional-scale erosional surface. Major facies associations of the Sequence I was Ephemeral Fluvial Channels mainly meandering deposits. Sequence I was interpreted to be a Type-I Falling Stage Systems Tract FSST) boundary marked by an unconformity. This was characterized by stream rejuvenation and fluvial incision, sedimentary bypass of the shelf, and abrupt basin-ward shift of facies and coastal onlap. This might be formed when the rate of eustatic fall exceeds the rate of basin subsidence at the depositional shoreline break, producing a relative fall in sea level below the position of the paleoshoreline [61].

3.4.1.1. Depositional architecture

Sequence I displayed a progradational facies succession. The base was dominated by fine-grained shallow marine deposits of the North Cape Formation that were overlain by fluvial strata. While fluvial flow was dominantly from NE to SW, indicating sediment transport towards the southern border of the basin.

Fluvial deposits were laterally and vertically adjacent, producing a complex depositional architecture. Both single storied and stacked meandering sand packages occur within the sequence consisting of 2-15m thick and >1 km in horizontal directions towards the X and Y axis of the model, the upper boundaries were fluvial scour surfaces with <5 m of erosional relief into the Aeolian deposits. Wherever single stack fluvial erosion was substantial, multiple channel deposits were severely to completely truncated (Fig.11).

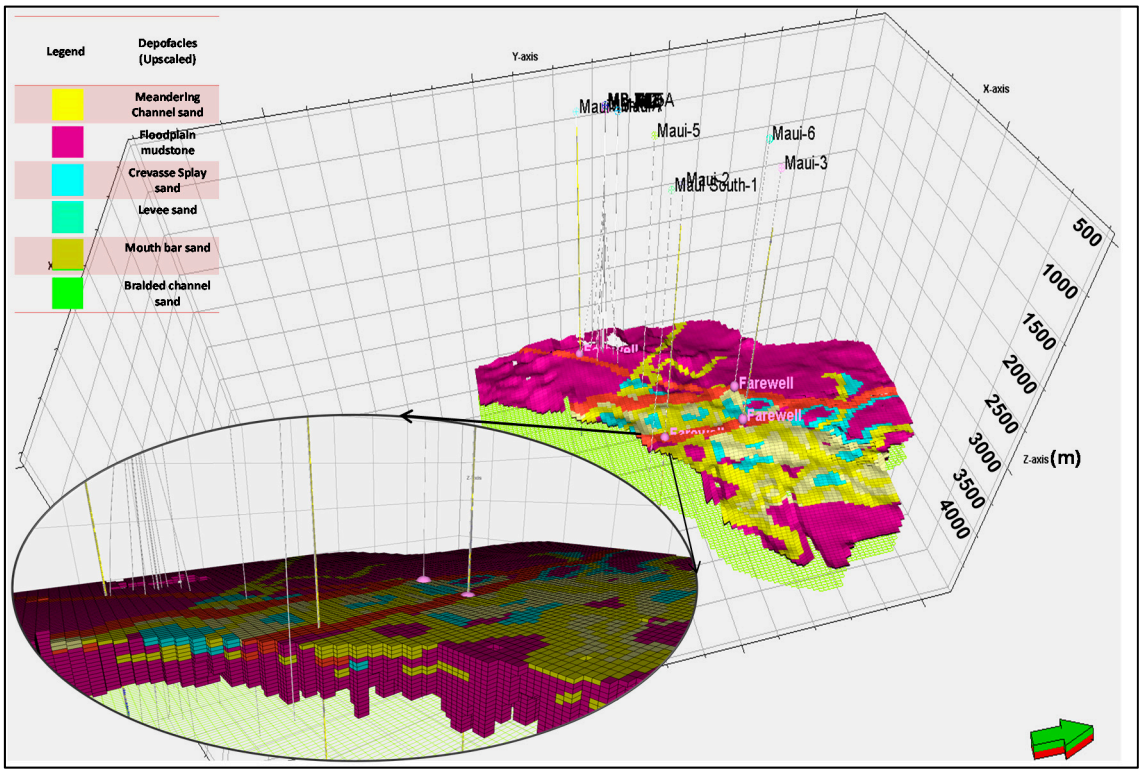

Figure.12. 3D geocellular facies distribution of the Farewell Formation. The image below represents the facies model in SIMBOX view, vividly displaying interpreted facies in X-Y-Z axis within the facies model of the Farewell Formation.

Preprints (www.preprints.org) | NOT PEER-REVIEWED | Posted: 15 January 2018 doi:10.20944/preprints201801.0123.v1

3.4.2. Sequence II

Sequence II ranged from 30-40 m in thickness. The lower boundary of Sequence II comprised a regional scale unconformity that was identified in the well logs and interpreted to be a Lowstand Systems Tract (LST) within the depositional cycles of the Farewell Formation. Its upper boundary was also defined by an erosional surface that can be correlated throughout the basin (Fig.11). Two facies associations were distinguished within this sequence, representing (1) Braided Fluvial Channel Belts and (2) Overbank Environments.

3.4.2.1. Depositional Architecture

Sequence II was uniform in terms of fluvial facies architecture throughout the entire basin, precluding the recognition of distinct internal stratigraphic intervals. This sequence represented a northwestward-flowing braided fluvial system developed on a widespread alluvial plain. Its geological record was characterized by a succession of sandstone bodies (braided channel belt deposits) partially separated by thin and discontinuous fine-grained, floodplain deposits. Therefore, Sequence II consisted of vertical and lateral juxtaposition of several sandstone bodies produced by successive avulsion episodes, similar to the fluvial accumulation models described elsewhere for braided fluvial systems [41, 68]. The minor quantity of flood plain deposits indicated that overbank sedimentation was either restricted or the resultant deposits were reworked by fluvial channels. The scarcity of mudstone intraclasts at the base of the sandstone bodies supported the former hypothesis, i.e. floodplains were poorly developed. Therefore sequence-II was interpreted to be regressive, being a Lowstand Systems Tract (LST).

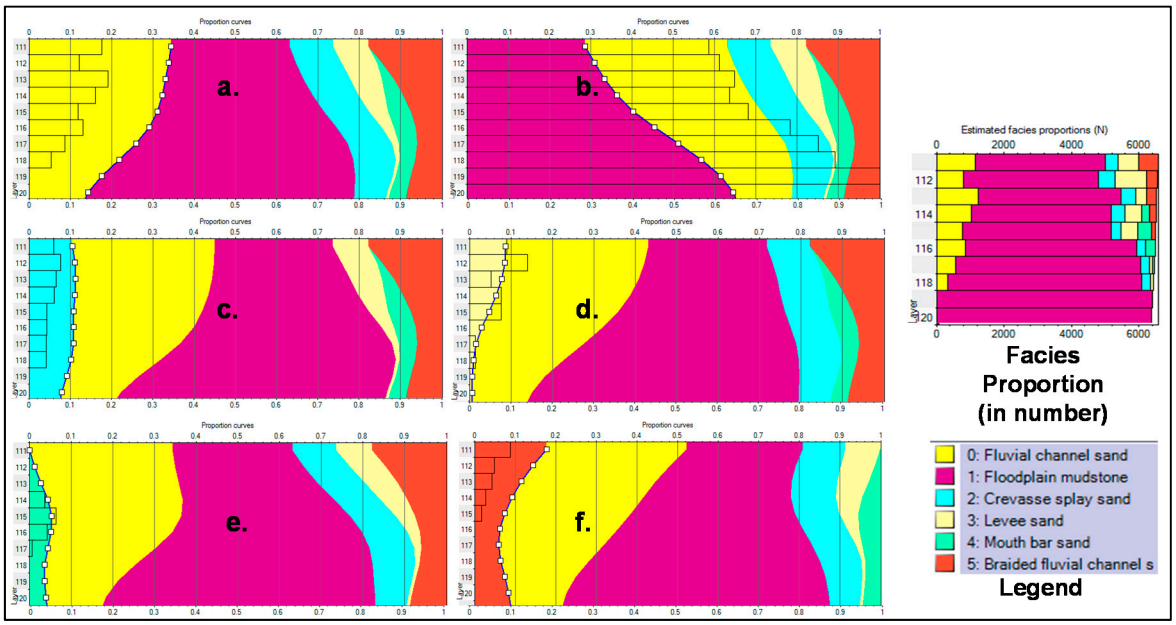

Figure.13. Vertical Proportion Curve (VPC) for all possible geobodies within the Farewell Formation. (a) VPC of fluvial (meandering) channel sands, (b) VPC of floodplain mudstone, (c) VPC of crevasse splay sands, (d) VPC of levee sand, (e) VPC of mouth bar sands, (f) VPC of braided channel sands.

3.5. 3D-Modeling Approach

The Facies Composite algorithm in Petrel was adopted to construct facies model of the Farewell Formation, which is an object-based facies modeling technique that can be used for a wide range of heterogeneities and depositional environments. The basic concept of the Facies Composite algorithm was that the facies within a grid model can be subdivided into a background facies and one or more object facies, which can have different shapes, sizes and orientations [22, 69-70]. The Facies Composite algorithm models the geometries and distribution of the object facies [23, 69, 71]. Facies sizes and shapes were drawn from a user-specified distribution that might differ locally within the reservoir [23, 72-74]. The entire process was based on a 3D geocellular modeling grid for the study and the discrete well data in a suitable format.

Preprints (www.preprints.org) | NOT PEER-REVIEWED | Posted: 15 January 2018 doi:10.20944/preprints201801.0123.v1

Following the structural restoration, the digital reconstruction of the boundaries of the sedimentary bodies involved the following steps: (a) visual construction of structured geobodies along with defined geometries of the interpreted lithology (b) variogram analysis of the geobody dimensions (c) incorporation of the paleo-depositional interpretation within each geobody and (d) construction of a consistent 3D subsurface-based model. The process of reconstructing the sedimentary bodies was used as a quality control on the existing field correlation. This reconstruction supported the interpreted rectilinear geometry of the channeled sandbodies.

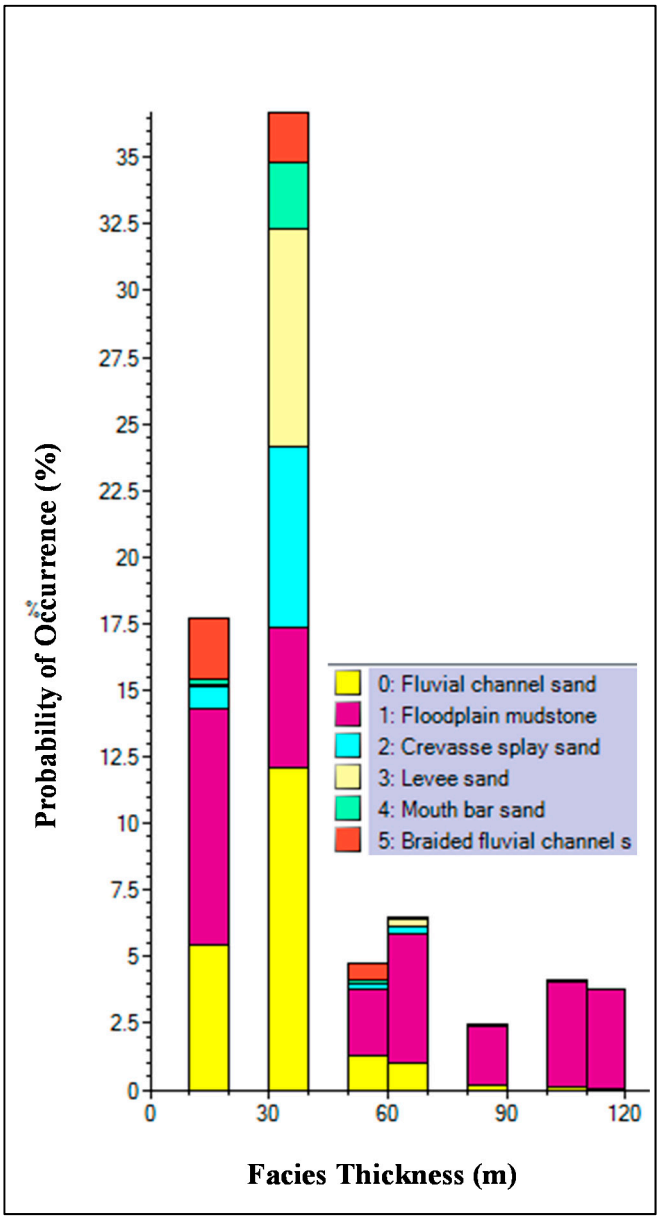

Figure.14. Facies proportions thickness Vs probability of occurrence for the Farewell Formation. Colors represent different geobodies interpreted in the model.

3.6. Modeling Grids and Constraints

For the 3D lithology models, seismic-derived structure maps were used to define the base and the top of the stratigraphic interval of the formation. The top of the model was then assigned within the layering algorithm denoting arbitrary layer number 110, and the base of the model being 120, which was around 100m in thickness on an average along the studied wells (Fig.12). Between the reservoir, 9 zones of equal thickness were constructed for better enhancement (along the vertical Z-axis) of the 3D facies grid. It was essential to define these zones within the reservoir interval to

 doi:10.20944/preprints201801.0123.v1

accurately model the lithologic variability within the reservoir. For the construction of the modeled grid, following process was used to create the vertical proportion curve.

A vertical proportion curve (VPC) (Fig.13) is a cumulative probability plot that shows the percentage of lithology versus depth. In this study we characterized VPC analysis considering all the studied wells within the gridded model. To create the vertical proportion curve, the interval between Farewell Formation was subdivided into an equal number of approximately 10m thick layers.

For this reason, proportional layers were defined within this stratigraphic interval in the well logs. The proportional layers had an approximate thickness of 10m in general but the thickness varied laterally, from well to well, given the same number of layers per reservoir zone on each well log. For each layer, the percentage of each lithology (sandstone, shale, coal) in that interval was determined from the well logs. The original well-log data were used in this analysis. By combining the well log data for each layer in this way, a vertical proportion curve was created that provides a 1D vertical trend to show how the lithology percentages vary with respect to depth in this study area.

From the VPC, it was evident that 6 different geobodies were three-dimensionally distributed along the Farewell Formation. From figure 13(a) meandering channel sand proportion curve was interpreted. We interpreted that, probability of occurrence for meandering channel sands were varying in different layers of the model. Layer 111-115 had higher probability of occurrence whereas layers from 116-118 have 20-29% probability of occurrence within the model. Layer 119-120 had only 10-15% probability of having meandering channel sand deposits. For floodplain mudstones, highest percentage of occurrence concentrated within the deeper layers (30-60%) (Fig.13b). For crevasse splay sands, probability of occurrence was very low; around 10% for all the interpreted layers of the Farewell Formation (Fig.13c). Figure 13d represented VPC for levee sands. Probability of occurrence for levee sands within the model was very low in the deeper layers (2-8%) compared to that of the shallower layers (5-9%). Mouth bar sands had a distribution of lower VPC all along the modeled layers (Fig.13e). Braided channel sands had higher probability of occurrence in the shallow layers, compared to the meadering ones.

To create the 3D model grid based on the VPC, facies thickness maps were generated for each of the reservoir zones. The isopach maps were added to a single reference surface in the model to create the additional structure maps (reservoir model surfaces) needed to define the 3D model grid or framework. This process ensured all structure maps to be consistent with the structural trends.

A detailed 3D facies model of 300,000 geo-gridded cells was created for 3D facies modeling. Fine-scale layers were distributed proportionally between the key stratigraphic surfaces. Each fine layer was approximately 10m thick to capture the stratigraphic detail of both meandering and braided deposits. Lateral cell dimensions of 50m X 50m were used to capture the details of the lateral distribution of the fluvial deposits and in order to have several cells between wells.

To honour the lithologic variability in wells, lithology logs were created for each well and subsequently upscaled to the resolution of the model grid and used in the modeling process. To create the lithology logs for all 4 wells, various cutoffs for the well-log data were used for each lithology for generating point attributes for each well, that later were incorporated into the 3D model. It was to be noted that in the study area, values less than 70 API units on the gamma-ray log was defined as sandstones (North and Boering 1999; Rider 1990). Values greater than 70-90 API units on the gamma-ray log was defined as silty sandstone to clayey siltstone and values above that were all termed as shales.

During the modeling process, the scaled sand-shale ratio volume was used as a conditioning parameter to control the spatial distribution of sandstone bodies or sandstone lithology within the 3D models. The calculations were performed using the Data Analysis plug-in of Petrel (Fig.14). As a result, if a modeled layer within the Farewell reservoir exhibits a high percentage of sandstone, the corresponding reservoir layer in the 3D model will have a high percentage of sandstone.

For the object-based lithology (sandstone, shale) modeling, the dimensions of sand bodies were derived from previous depositional and paleo-depositional studies performed on the basin [23,

Preprints (www.preprints.org) | NOT PEER-REVIEWED | Posted: 15 January 2018 doi:10.20944/preprints201801.0123.v1

75-78]. For the indicator based modeling, the spatial correlation of the lithologies of the Farewell Formation was quantitatively analyzed through variogram analysis. Experimental variograms were calculated separately for each reservoir zone and lithology and were fitted with exponential and spherical variogram models. Correlation lengths of the model variograms ranged from approximately 25-35000 m parallel to paleoflow (Northeast to Southwest) in the major direction and

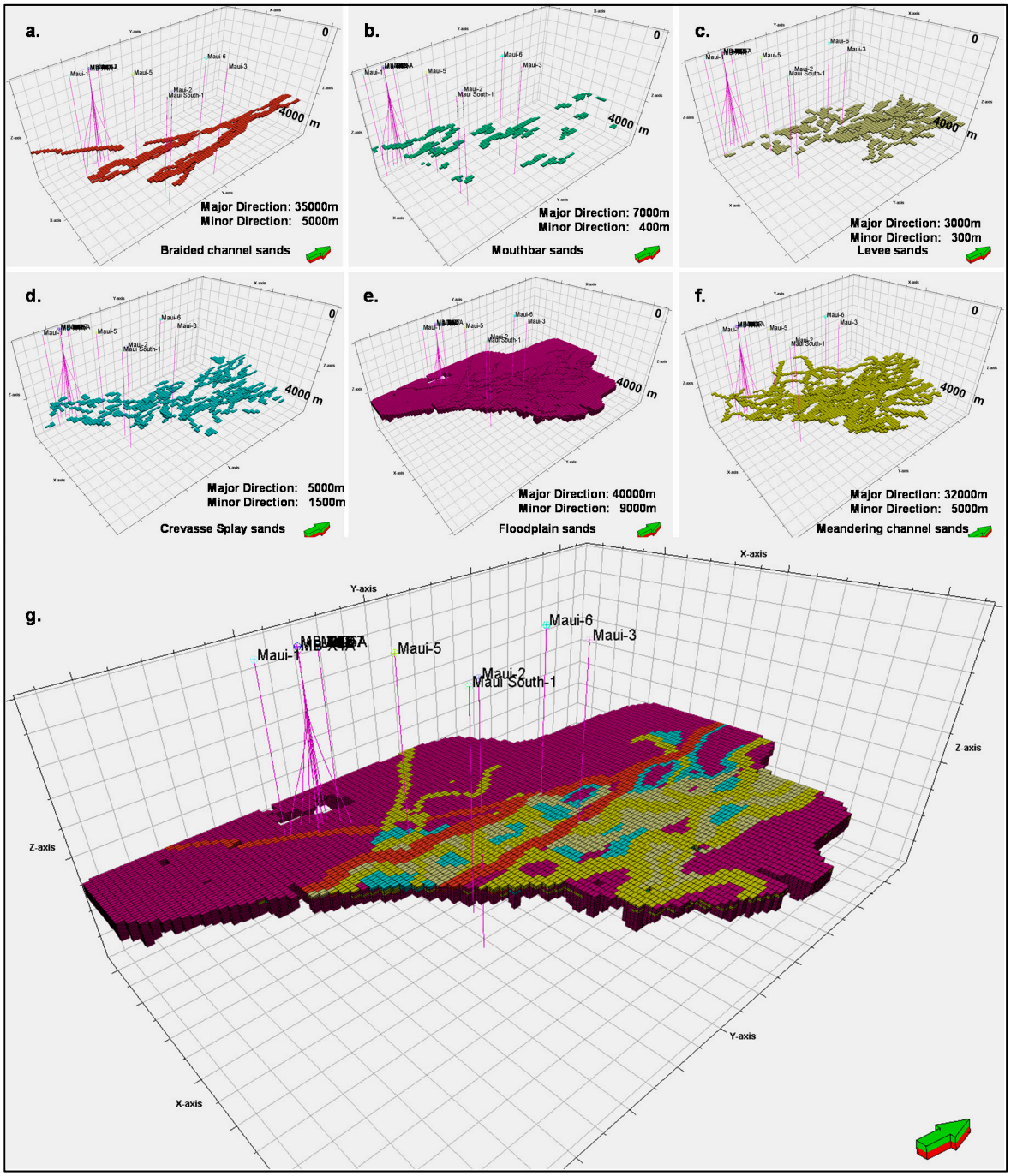

Figure.15. Object geometries (a-f) of the interpreted geobodies of the Farewell Formation. Each geobody represents its spatial distribution within the formation along the X-Y-Z axis of the modeled grid. Braided channel sands to meandering channel deposits have been modeled for the analysis. Figure 15g represent the entire facies model combined with all possible geobodies of the Farewell Formation, Maui Gas Field.

around 12-15000 m perpendicular to paleoflow in the minor direction and vertically around 100 m on an average within the studied wells (Fig.15). The few zones with longer vertical correlation lengths appeared to correspond to stacked mouth-bar deposits (multistory channel-fill deposits)

 doi:10.20944/preprints201801.0123.v1

rather than individual mouth bars. It was important to note that the correlation lengths do not directly provide information on the dimensions, geometry and sinuosity of the fluvial deposits.

We used sequential-indicator simulation and conditioned it to fit with the object based geobody modeling [30, 75] to generate a 3D facies model for the Farewell Formation. A value for lithology was simulated in each cell of the model based on probabilities calculated from well data and user-defined inputs. The percentages of each lithology were defined for each zone based on well data.

For the sequential-indicator simulation model (indicator-based model), the global volume fraction for sandstone was 45% sandstone and 55% shale. Because indicator-based simulation used variograms (a two-point statistics) to incorporate the spatial correlation of the reservoir lithologies, the geometries of channel sand bars were, as expected, not reproduced using this method. However, the general distribution of sandstone honored all the constraints. The lower portion of the facies model (layer 115-120) of the indicator-based model was composed primarily of discontinuous sandstones and shales which whereas stacked and more continuous sandstone and interbedded shale intervals were more common in the upper part of the facies model. The upper part was therefore denominated as possible braided stacked channel sands and the lower being multistoried meandering channel sand deposits. Relatively small and discontinuous sand bodies were observed throughout the modeled interval.

3.7. Object geometry

The geometrical properties for each selected facies association in all zones were set by defining different and reasonable geometries (Fig.15a-f). Distributary channel, the main H/C bearing facies, was defined as a backbone which was a variant of the axial shape where the object was deformed locally to follow a direction parameter. Its thickness and width remained constant along axis and the cross sectional formed as U shapes (Fig.15f). The overbank was also defined as an axial shape with constant thickness and slight width variation. The mouth bar (Fig.15b) was defined as an axial lobe body whose width increased then decreased along axis with a lentoid cross sectional form. It was worth noting that these definitions do not determine the size or orientation of the bodies, they only specify a prototype shape for the object and this shape was then rescaled and orientated using the size and orientation attribute values.

Evidence of possible multi-storey stacking within the sand-body profile was usually in the form of a minor gamma peaks that might result from thin units of fine-grained sediment or, more likely, horizons of intra-formational mud clasts resting on erosion surfaces at the bases of stacked storeys. Such sandbodies range in thickness from around 10 m up to over 20 m (Fig.15a/f). In the object-based facies modeling, it was necessary to define facies body log to split a multi-storey channel interval into different facies objects and get a better statistics of properties and thus a better simulation result [79-80]. The body division results were showed along with the prospective major and minor directions in figure 15 (a-f).

3.8. Object-based simulation of the geobodies

Object-based simulation involves defining lithology (or facies, architectural element) objects with a range of dimensions and characteristic shapes that were used to populate the 3D model [80-81]. This method honored geologic rules for stacking patterns and erosion and user-defined shapes that, in some cases, can produce more geologically realistic models than other modeling methods [30, 75].

For this study, the modeled elements were crescent-shaped objects that represent the main reservoir elements (mouth bars) within the studied formation. The thickness of individual channel sands within the grid was modeled using a triangular distribution with values ranging from 2-15m with an average of 8.5m. Individual bar widths range from 200-400m with an average of 300m. The mouth-bar shape was modeled as a scalable crescent-shaped body based on the study of paleo-channel reconstructions of mouth bars [23, 77-78]. Therefore this method used objects with distinct shapes to control the spatial continuity and distribution of lithologies (i.e., variograms were

Preprints (www.preprints.org) | NOT PEER-REVIEWED | Posted: 15 January 2018 doi:10.20944/preprints201801.0123.v1

not used) which resulted in improved model predictions as compared to the corresponding indicator-based models.

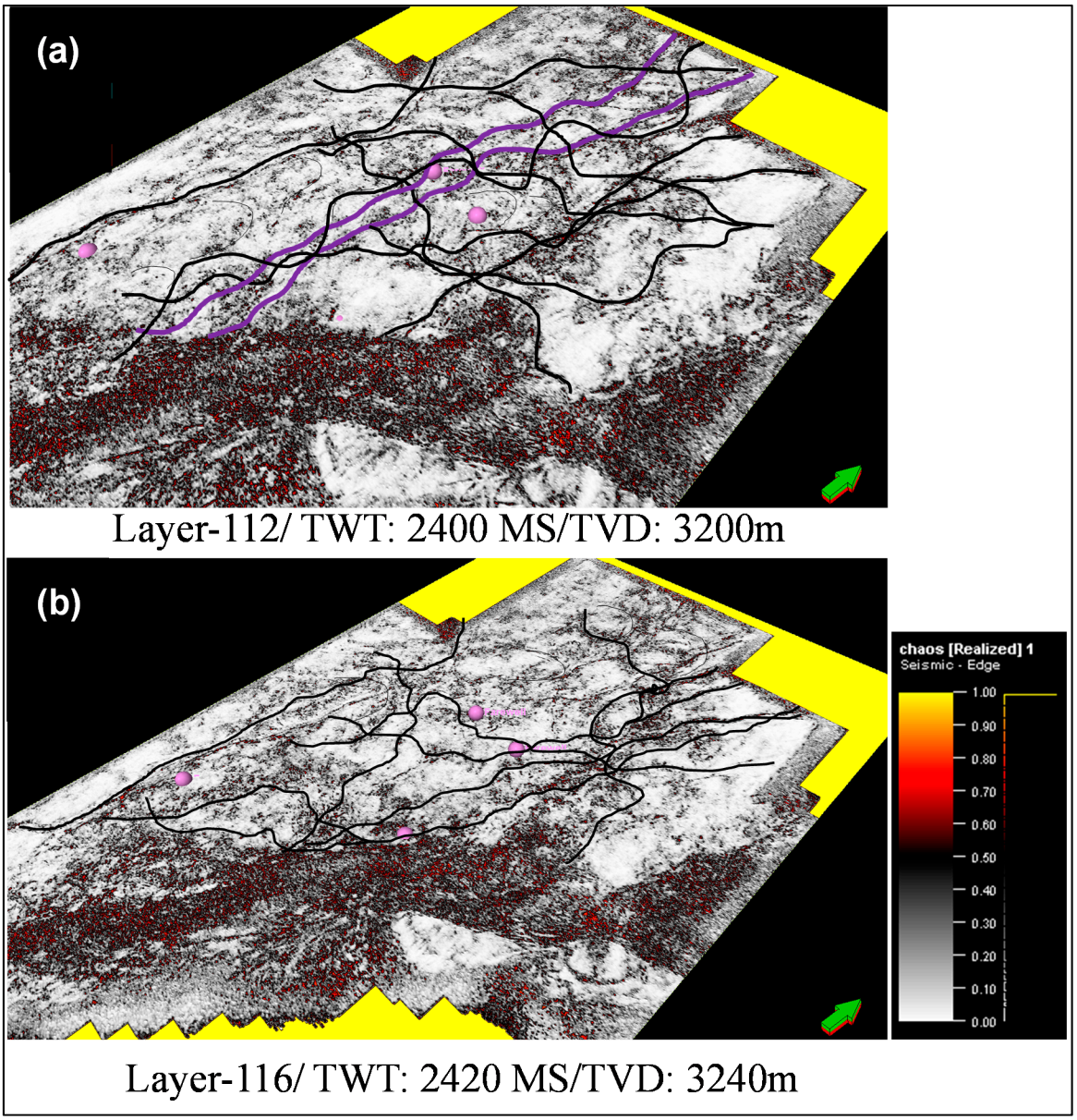

Figure.16. Seismic attribute (coherence) showing the paleochannels within the Farewell Formation. Solid black lines are possible fluvial channels as interpreted on the Z slice of the seismic cube.

To simplify the modeling process, separate stochastic object-based models were generated for each lithology and then merged to create the final lithology model. The two sandstone and shale models were constructed using the same ranges of object dimensions for the sandstone bodies but used different object orientations. These models were then merged to create a final model with point orientations that were consistent with outcrop measurements. The orientations of the geobodies were consistent with the approximate paleoflow direction of the Farewell Formation of the Maui Gas Field. The range in orientations produced crescent-shaped and lenticular objects that represent bar deposits on opposite sides of a sinuous meandering stream system. Using this approach, crescent-shaped sand bar objects were modeled, along with the fluvial channels; therefore, the sinuosity, amplitude and wavelength of the inferred channels that deposited the sandstones were not used as input into the modeling process. The sinuosity of Farewell Formation fluvial channels was estimated to be approximately 1.7–1.9 based on sandstone body width-to-thickness ratios and paleo channel direction measurements from the 3D seismic cube [31, 82]. Although channel

Preprints (www.preprints.org) | NOT PEER-REVIEWED | Posted: 15 January 2018 doi:10.20944/preprints201801.0123.v1

amplitude and wavelength were not modeled explicitly, the modeled object dimensions and orientations were consistent with the previous studies [23, 31, 77, 82]. With the combination of indicator and object based modeling, the final outputs were constrained by well data and seismic picks and resulted in a 3D geobody grid for the studied formation.

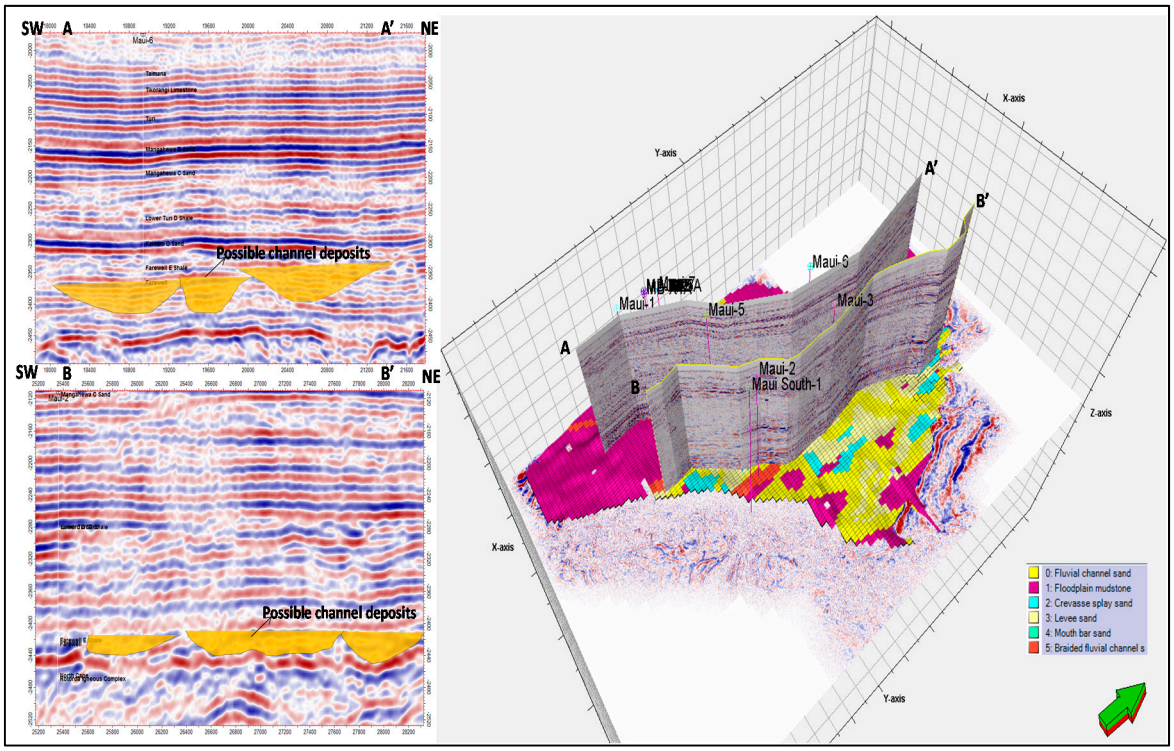

Figure.17. Vertical seismic profiles (in TWT) for the Farewell Formation. AA' and BB' profiles represent major channel forms along the facies model of the formation. Note that the interpreted paleochannels (BB') have more width-thickness ratio compared that of the westward profile (AA').

3.9. 3D Facies Architecture based on Seismo-sedimentological Interpretation

A number of investigations were published on facies architecture analysis based on outcrop, well, seismic, and experimental data [45, 52, 83-87]. In this study, we applied seismic sedimentology to extend the well data study to the entire block covered by 3-D seismic survey and to provide more detailed sedimentary facies architecture mapping [29, 88-90]. Stratal slicing and 90°-phasing were two key techniques used in seismic sedimentology analysis [29, 89].

Using horizontal seismic patterns within a small travel-time window that followed the sedimentary facies, a stratal slice could reveal more detailed geobody distributions and sedimentary facies in much higher resolution with less ambiguity than that was possible by using classic seismic stratigraphy [89-90].

3.9.1. Spatial distribution and temporal evolution of incised valleys

The incised valley fill was used to identify the sediment transport direction, deduce the sedimentary dispersal system, and served as a potential high-quality reservoir [91-94]. As a typical sand-prone fill and the main drainage system in the study area, the spatial distribution and temporal evolution of incised valleys were investigated in great detail.

3.9.1.1. Spatial distribution of incised valleys

Figure 16 explained the spatial distribution of incised valleys using coherence attribute. Coherence attribute was used in the study because of its effectiveness in identifying edge detection along with possible channel boundaries. In figure 16a to figure 16b, the bottom of each figure was the stratal slice showing the reflection amplitude of the bottom boundary of sequence II; in inline

Preprints (www.preprints.org) | NOT PEER-REVIEWED | Posted: 15 January 2018 doi:10.20944/preprints201801.0123.v1

and crossline cross sections, respectively, which were used for interpreting the spatial distribution of incised valleys.

Moving the Z slices on the seismic sections from figure 16a to 16b, the numbers of incised valleys changes and their width-to-thickness ratio was evident from upstream to downstream region of the stratal slice(Fig.16). In figure 16a, at least 9 prominent incised valley fills were interpreted on the seismic section with multiple, very strong converging and branching belt-shaped amplitude anomalies in the slice from upstream to downstream (NE-SW). The anomalies had a close corresponding relationship with incised valleys on the seismic section, indicating the planar distribution of multiple incised valleys.

11 incised valleys were interpreted in figure 16b. There were also combined channel forms, branching out from main channel seen in the seismic slice. This corresponds to high amplitude anomalies (coherence attribute) in the stratal slice. It was also evident that the width-to-thickness ratio of incised valleys gradually decreases from upstream to downstream.

3.9.1.2 Temporal evolution of incised valley fills

Representative seismic profiles shown in 3-D visualization from the Farewell Formation sequences revealed the temporal evolution of the incised valley fills from the bottom to top boundary (Fig.17). In figure 17, the bottom of the illustration was the vertical slice showing the reflection amplitude of different stages of the two major sequences. The higher amplitudes were characterized by channel sands distributed spatially.

The belt-shaped high amplitudes reflected the difference of incised valley fills in the stratal slices, indicating the differences in width, sinuosity, continuity, and extended length (Fig.17), reflecting the hydrodynamic change and temporal evolution of an incised valley fill. The incised valleys tend to be of broad and straight amplitude anomalies. In comparison, it was observed that incised valleys were characterized by narrow and meandering channels; the number of incised valleys obviously increases while their width decreases. The incised valleys actively developed in figure 17 were almost faded in the bottom vertical slice; whereas incised valleys developed at the top slice were characterized by branching and converging. From the interpretation of channel distribution and occurrence, the variations in number, width, and sinuosity of incised valleys indicated the evolution of incised valleys from initiation to extinction [91, 94-95].

5. Conclusions

The following conclusions can be made from this study:-

1) We identified three major depositional facies distributed over the paleo-environmental setup of the Farewell Formation. It was also observed that the current workflow of facies occurrence and probability according to the geological knowledge-base and grid sequencing showed considerable improvements within the modeled region of the Maui Gas Field.

(2) The Farewell reservoir was interpreted to be of fluvial paleo-environment in origin. Interpretations lead us to believe that about 45% of the depositional facies are of channel sandstone origin and the rest 55% are floodplain/overbank shales.

(3) The Farewell model was sequence stratigraphically interpreted to be of Type-I origin having Lowstand Systems Tract (LST) of fluvial origin.

(4) It was also observed that the lower portion of the geobody facies model (layer 115-120) was composed primarily of discontinuous sandstones and shales. Sandstone and interbedded shale intervals were more common in the upper part of the facies model. The upper part was therefore denominated as possible braided stacked channel sands and the lower being multistoried meandering channel sand deposits.

(5) We modeled at least eleven prominent incised valley fills on the seismic section with multiple, very strong converging and branching belt-shaped amplitude anomalies in the slice from upstream to downstream (NE-SW). The anomalies had close corresponding relationship with incised valleys on the seismic section, indicating the planar distribution of multiple incised valleys.

There were combined channel-forms, branching out from main channel corresponding to high amplitude anomalies predicted to be higher quality reservoir sands.

(6) The geobody modeling process had effective advantage of quantitative propagation of uncertainty via the object-based algorithm of the identified geobodies distributed across of the formation. Thus the facies model was interpreted to be used as a significant new tool for future studies on deeper reservoirs and their development strategies for better production.

Acknowledgments: This study is funded as part of the doctoral research (GRS-2015) at the Department of Geological Sciences, Universiti Brunei Darussalam (UBD). The authors would like to thank Ministry of Business, Innovation and Employment (MBIE), New Zealand for providing dataset containing 3D seismic, well logs and associated reports required for this study. Schlumberger is greatly acknowledged for supporting us with Petrel G&G software v.2013.1.

Author Contributions: AKM Eahsanul Haque (A. E. H.) developed the 3D geobody modeling concept for the reservoir, workflow and static modeling parameters; Md Aminul Islam (M. A. I.) improved the well log facies analysis and Mohamed Ragab Shalaby (M. R. S.) contributed to correct the manuscript.

Conflicts of Interest: The authors declare no conflict of interest.

References

1. 1. Childs, C.; Nicol A.; Walsh J. J. The growth and propagation of synsdimentary faults. *Journal of Structural Geology* **2003**, 25(4), 633–648, doi.org/10.1016/S0191-8141(02)00054-8.
2. Reilly, C.; Nicol A.; Walsh J. J. Evolution of faulting and plate boundary deformation in the Southern Taranaki Basin, New Zealand. *Tectonophysics* **2015**, 651, 1–18, doi.org/10.1016/j.tecto.2015.02.009.
3. Uruski, C. I. Deepwater Taranaki, New Zealand: structural development and petroleum potential. *Exploration Geophysics* **2008**, 39(2), 94-107, doi.org/10.1071/EG08013.
4. Mcbeath, D. M. Gas-condensate fields of the Taranaki basin, New Zealand. *New Zealand Journal of Geology and Geophysics* **1977**, 20(1), 99–127.
5. Kamp, P. J. J.; Vonk, A, J., Bland, K. J.; Hansen, R. J.; Hendy, A. J. W.; Mcintyre, A. P.; Ngatai, M.; Cartwright, S. J.; Hayton, S.; Nelson, C. S. Neogene stratigraphic architecture and tectonic evolution of Wanganui, King Country, and eastern Taranaki Basins, New Zealand. *New Zealand Journal of Geology and Geophysics* **2004**, 47(4): 625-644, doi.org/10.1080/00288306.2004.9515080.
6. King, P. R.; Thrasher, G. P. Cretaceous–Cenozoic geology and petroleum systems of the Taranaki Basin, New Zealand. Institute of Geological and Nuclear Sciences, Lower Hutt, New Zealand, 1996, 13(2).
7. King, P. R. Polyphase evolution of the Taranaki Basin, New Zealand: changes in sedimentary and Structural style. New Zealand Oil Exploration Conference Proceedings, Wellington, 1990, 134–150.
8. King, P. R.; Browne, G. H.; Slatt, R. M.; Diridoni, J. L. High resolution sequence stratigraphy of Miocene Deepwater clastic outcrops, Taranaki coast, New Zealand. American Association of Petroleum Geologists International Conference and Exhibition, 1995, 79, CONF-950995.
9. Skalle, P.; Aamodt, A. Knowledge-based decision support in oil well drilling. International Conference on Intelligent Information Processing, 2004, 443-455.
10. Luthi, S. (2001). Geological well logs: Their use in reservoir modeling. Springer Science & Business Media, 2001.
11. Higgs, K. E.; Funnell, R. H.; Reyes, A. G. Changes in reservoir heterogeneity and quality as a response to high partial pressures of CO 2 in a gas reservoir, New Zealand. *Marine and Petroleum Geology* **2013**, 48, 293-322, doi.org/10.1016/j.marpetgeo.2013.08.005.
12. Higgs, K. E.; Zwingmann, H.; Reyes, A. G.; Funnell, R. H. Diagenesis, porosity evolution, and petroleum emplacement in tight gas reservoirs, Taranaki Basin, New Zealand. *Journal of Sedimentary Research* **2007**, 77(12), 1003-1025, doi.org/10.2110/jsr.2007.095.
13. Martin, K. R.; Baker, J. C.; Hamilton, P. J.; Thrasher, G. P. Diagenesis and reservoir quality of paleocene sandstones in the Kupe South field, Taranaki Basin, New Zealand. *AAPG bulletin* **1994**, 78(4), 624-643.
14. Strogen D. P.; Bland K. J.; Baur J. R. Rift to drift on the edge of Gondwana: Cretaceous-Eocene paleogeographic evolution of the Taranaki Basin, New Zealand. Geosciences New Zealand Annual conference, Wellington, New Zealand, 2014, 1–17.
15. Laird, M. G. Cretaceous continental rifts: New Zealand region. *Sedimentary basins of the world* **1993**, 2, 37-49..

16. Stagpoole, V. M.; Nicol A. Regional structure and kine-matic history of a large subduction back thrust: Taranaki Fault, New Zealand. *Journal of Geology and Geophysics* **2008**, 113(B1), 769–775, doi.org/10.1029/2007JB005170.
17. Holt, W. E.; Stern T. A. Subduction, platform subsidence, and foreland thrust loading: The late Tertiary development of Taranaki Basin, New Zealand. *Tectonics* **1994**, 13(5), 1068–1092, doi.org/10.1029/94TC00454.
18. King, P. R.; Thrasher G. P. Post-Eocene development of the Taranaki Basin, New Zealand: Convergent overprint of a passive margin. Geology and geophysics of continental margins **1992**, 53, 93–118.
19. Bussell, M. R. Seismic interpretation of the Moki Formation on the Maui 3D survey, Taranaki Basin. New Zealand Petroleum Conference proceedings, Sydney, Australia, 1994, 240-255.
20. King, P. R.; Robinson, P. R. An overview of Taranaki region geology, New Zealand. *Energy Exploration & Exploitation* **1988**, 6(3), 213–232.
21. Haque, A. E.; Islam, M. A.; Shalaby, M. R. Structural Modeling of the Maui Gas Field, Taranaki Basin, New Zealand. *Journal of Petroleum Exploration and Development* **2016**, 43(6), 965-975, doi.org/10.1016/S1876-3804(16)30114-8.
22. Pyrcz, M. J.; Mchargue, T.; Clark J.; Sullivan, M.; Strebelle, S. Event-based geostatistical Modeling: description and applications. *Geostatistics* 2012, 27-38, doi.org/10.1007/978-94-007-4153-9_3.
23. Pyrcz, M. J.; Sech R. P.; Covault, J. A.; Willis, B. J.; Sylvester, Z.; Sun, T. Stratigraphic rule-based reservoir modeling. *Bulletin of Canadian Petroleum Geology* **2015**, 63(4): 287-303.
24. Keeton, G. I.; Pranter, M. J.; Cole, R. D.; Edmund, R. Stratigraphic architecture of fluvial deposits from borehole images, spectral-gamma-ray response, and outcrop analogs, Piceance Basin, Colorado. *AAPG Bulletin* **2015**, 99(10), 1929-1956.
25. Deutsch, C. V. Geostatistical Reservoir Modelling, Oxford University Press, 2002, pp. 376.
26. Strebelle, S.; Zhang T. Non-stationary multiple-point geostatistical models. *Geostatistics Banff 2004* **2005** 235-244.
27. Goovaerts, P. (2006). Geostatistical modeling of the spaces of local, spatial, and response uncertainty for continuous petrophysical properties. In *Stochastic modeling and geostatistics: Principles, methods, and case studies, volume II: AAPG Computer Applications in Geology*; T. C. Coburn, T. C.; Yarus, J. M.; Chambers, R. L, AAPG, USA, 2007; 2(5), pp. 59–79, doi.org/10.1306/1063807CA53229.
28. Mikes, D.; Barzandji, O. H. M.; Bruining, J.; Geel, C.R. Upscaling of small-scale heterogeneities to flow units for reservoir modeling. *Mar. Pet. Geol.* **2006,** 23(9), 931-942, doi.org/10.1016/j.marpetgeo.2005.06.005.
29. Zhang, T.; Zhang, X.; Lin, C.; Yu, J.; Zhang, S. Seismic sedimentology interpretation method of meandering fluvial reservoir: From model to real data. *Journal of Earth Science* **2015**, 26(4):598-606, doi.org/10.1007/s12583-015-0572-5.
30. Deutsch, C. V.; Journel A. G. Geostatistical Software Library and user's guide, Oxford University Press, New York, pp. 369.
31. Pranter, M. J.; Ellison A. I.; Cole R. D.; Patterson P. E. Analysis and modelling of intermediate-scale reservoir heterogeneity based on a fluvial point-bar outcrop analogue, Williams Fork Formation, Piceance Basin, Colorado. *AAPG Bulletin* **2007**, 91(7), 1025–51, doi.org/ 10.1306/02010706102.
32. Bal, A. A. Estuarine to fluvial transition: the Cretaceous/Tertiary "Puponga" Coal Measures in the Pakawau Group, northwest Nelson. B.Sc (Hons) thesis, University of Canterbury, New Zealand, 1992.
33. Bal, A. A. (1994). Cessation of Tasman Sea spreading recorded as a sequence stratigraphy: interpretation of an early Paleocene unconformity in the Pakawau subbasin, NW Nelson, New Zealand. In The evolution of the Tasman Sea Basin, Proceedings of the Tasman Sea Conference, Christchurch, New Zealand, 1994, Van der Lingen, G. J.; Swanson, K. M.; Muir, R. J. Balkema Publishers, pp. 23-30.
34. Bal, A. A. Disparate hydrocarbon generation potential and maturation profiles of Pakawau Group source coals: implications for Taranaki Basin exploration, New Zealand. In Petroleum Exploration Conference Proceedings, Ministry of Economic Development, Wellington, New Zealand, 1994, pp. 322–337.
35. Thrasher, G. P. Late Cretaceous source rocks of Taranaki Basin. New Zealand Oil Exploration Conference proceedings, Crown Operations Group, Energy and Resources Division, 1991, pp. 147-154.
36. Benvenuti, M.; Del C., S. Facies and sequence stratigraphic modeling of a Upper Pliocene–Lower Pleistocene fluvial succession (Valdelsa Basin, central Italy). *Sedimentary Geology* **2013**, 294, 303–314, doi.org/10.1016/j.sedgeo.2013.06.006.

37. Fanti, F.; Catuneanu, O. Fluvial sequence stratigraphy: the wapiti Formation,West- Central Alberta, Canada. *Journal of Sedimentary Research* **2010**, 80(4), 320–338.
38. Chakraborty, T. Reconstruction of fluvial bars from the Proterozoic Mancheral Quartzite, Pranhita–Godavari, India. In *Fluvial Sedimentology VI,* Int. Assoc. Sediment. Special Publication, 1999, 28, pp. 451–466.
39. Miall, A. D. Facies architecture in clastic sedimentary basins. *New perspectives in basin analysis* ***1988***, 67-81.
40. Miall, A. D. Reservoir heterogeneities in fluvial sandstones: lessons from outcrop studies. *AAPG Bulletin* **1988**, 72(6), 682-97.
41. Miall, A. D. The Geology of Fluvial Deposits: Sedimentary Facies, Basin Analysis and Petroleum Geology. Springer-Verlag, New York, USA, 2013, pp. 495-519.
42. North, C. P., Taylor, K. S. Ephemeral–fluvial deposits: integrated outcrop and simulation studies reveal complexity. *AAPG Bulletin* **1996**, 80(6), 811–830,
43. Aitken, J. F.; Flint, S. The application of sequence stratigraphy to fluvial systems: an example from the Late Carboniferous of the Appalachians. *Sedimentology* **1995**, 42, 3–30.
44. Bristow, C.S. Brahmaputra river: channel migration and deposition. In *Recent Developments in Fluvial Sedimentology*, Ethridge, F.G.; Flores, R. M.; Harvey, M. D, SEPM Special Publication, 1987, 39, pp. 83–91.
45. Scherer, C. M.; Lavina E. L.; Dias F. D. C.; Oliveira F. M.; Bongiolo D. E.; Aguiar E. S. Stratigraphy and facies architecture of the fluvial–aeolian–lacustrine Sergi Formation (Upper Jurassic), Recôncavo Basin, Brazil. *Sedimentary Geology* **2007**, 194(3), 169-193, doi.org/10.1016/j.sedgeo.2006.06.002.
46. Gulliford, A.R.; Flint, S.S.; Hodgson, D.M. Testing applicability of models of distributive fluvial systems or trunk rivers in ephemeral systems: reconstructing 3-D fluvial architecture in the Beaufort Group, South Africa. *Journal of Sedimentary Research* **2014**, *84*(12), 1147-1169, doi.org/10.2110/jsr.2014.88.
47. Ékes, C. Bedload-transported pedogenic mud aggregates in the Lower Old Red Sandstone in southwest Wales. *Journal of the Geological Society* **1989**, 150(3), 469-71.
48. Rust, B. R,; Nanson G. C. Bedload transport of mud as pedogenic aggregates in modern and ancient rivers. *Sedimentology* **1989**, 36(2), 291-306.
49. Fielding, C. R.; Allen J. P.; Alexander J.; Gibling M. R. Facies model for fluvial systems in the seasonal tropics and subtropics. *Geology* **20009**, 37(7), 623-6.
50. Bridge, J. S. Description and interpretation of fluvial deposits: a critical perspective. *Sedimentology* **1993**, 40(4), 801-810.
51. Sahoo, H.; Gani, M. R.; Hampson, G. J.; Gani, N. D.; Ranson, A. Facies-to sandbody-scale heterogeneity in a tight-gas fluvial reservoir analog: Blackhawk Formation, Wasatch Plateau, Utah, USA. *Marine and Petroleum Geology* **2016**, *78*, 48-69, doi.org/10.1016/j.marpetgeo.2016.02.005.
52. Blum, M. Scaling relationships between fluvial channel fills, channel-belt sand bodies and drainage basins, with implications for the Mannville Group, Alberta Foreland Basin. AAPG Annual Convention and Exhibition, 2015.
53. Pisel, J. R.; Pyles D. R. On The Relationship Between Fluvial Channel-Belt Morphology And Internal Heterogeneity: Insights From Satellite, Seismic, Numerical, And Outcrop Datasets. Doctor of Philosophy Thesis, Colorado School of Mines, USA, 2015..
54. Willis, B. J.; Sech R.; Sun T.; Pyrcz M. Predicting Facies Patterns within Fluvial Channel Belts. Inagu Fall Meeting Abstracts, 2014, 1, 3529.
55. Godin, P. D. Fining-upward cycles in the sandy braided-river deposits of the Westwater Canyon Member (Upper Jurassic), Morrison Formation, New Mexico. *Sedimentary Geology* **1991**, 70(1), 61-82.
56. Colombera, L.; Mountney N. P.; Felletti F.; mccaffrey W. D. Models for guiding and ranking well-to-well correlations of channel bodies in fluvial reservoirs. *AAPG Bulletin* **2014**, 98(10), 1943-1965, doi.org/10.1306/05061413153.
57. Lowe, D. G.; Arnott R. W. Composition and Architecture of Braided and Sheetflood-Dominated Ephemeral Fluvial Strata In the Cambrian–Ordovician Potsdam Group: A Case Example of the Morphodynamics of Early Phanerozoic Fluvial Systems and Climate Change. *Journal of Sedimentary Research* **2016**, 86(6), 587-612, doi.org/10.2110/jsr.2016.39.
58. Van Wagoner, J. C.; Mitchum R. M.; Campion K. M.; Rahmanian V. D. Siliciclastic sequence stratigraphy in well logs, cores, and outcrops: concepts for high-resolution correlation of time and facies, AAPG Methods in Exploration, 1990, 7, 55.

59. Posamentier, H. W.; Weimer P. Siliciclastic Sequence Stratigraphy and Petroleum Geology--Where to From Here?: *AAPG Bulletin* **1993**, 77(5), 731-742.
60. Zecchin M.; Catuneanu, O. High-resolution sequence stratigraphy of clastic shelves III: applications to reservoir geology. *Marine and Petroleum Geology* **2015**, 62, 161-175, doi.org/10.1016/j.marpetgeo.2014.08.025.
61. Catuneanu, O., Zecchin M. Comment on "Non-unique stratal geometries: implications for sequence stratigraphic interpretations", by: PM Burgess and GD Prince. *Basin Research* **2017**, 29(5), 625-629, doi.org/10.1111/bre.12192.
62. Miall, A. D. Stratigraphy: The Modern Synthesis. In *Stratigraphy: A Modern Synthesis*, 2016, 311-370.
63. Reijenstein, H. M., Posamentier H. W., Fantin M., González T. F., Lipinski C. (2014). Vaca Muerta Seismic stratigraphy and Geomorphology: regional architectural trends for unconventional exploration. Inix Congreso de Exploración y Desarrollo de Hidrocarburos IAPG, Mendoza, Argentina.
64. Reuter, M., Auer G., Brandano M., Harzhauser M., Corda L., Piller W. E. (2017). Post-rift sequence architecture and stratigraphy in the Oligo–Miocene Sardinia Rift (Western Mediterranean Sea). Marine and Petroleum Geology, 79:44-63.
65. Shanley, K. W.; Mccabe, P. J. Perspectives on the sequence stratigraphy of continental strata. *AAPG Bulletin* **1994**, 78(4), 544-568,
66. Wright, V. P.; Marriott, S. B. The sequence stratigraphy of fluvial depositional systems: the role of floodplain sediment storage. *Sedimentary Geology* **1993**, 86(3-4), 203-210, doi.org/10.1016/0037-0738(93)90022-W.
67. Miall, A. D.; Arush, M. Cryptic sequence boundaries in braided fluvial successions: *Sedimentology* **2001**, 48(5), 971-985, doi.org/10.1046/j.1365-3091.2001.00404.x.
68. Jones, H. L.; Schumm, S. A. Causes of avulsion: an overview. In *Fluvial Sedimentology VI,* Blackwell Publishing Ltd Oxford, UK, **1999**, 28, pp. 171–178.
69. Pyrcz, M. J.; Deutsch C. V. Geostatistical reservoir modeling. Oxford university press, 2014.
70. Seifert, D.; Jensen, J. L. Object and pixel-based reservoir modeling of a braided fluvial reservoir: *Mathematical Geology* **2000**, 32(5), 581– 603, doi.org/10.1023/A:1007562221431.
71. Bayer, P.; Comunian A.; Höyng D.; Mariethoz G. High resolution multi-facies realizations of sedimentary reservoir and aquifer analogs. *Scientific data 2* **2015**, doi.org/10.1038/sdata.2015.33.
72. Torres, J. A. Approaches to Integrate Seismic Data into Geocellular Modeling, Angsi Field Case Study. Seismic Driven Reservoir Characterization and Production Management Meeting, 2015, doi.org/10.3997/2214-4609.201412295.
73. Barboza, S. A.; Alway, R.; Akpulat, T.; Esch, W. L.; Hicks, P. J.; Gerdes, M. L. Stochastic Evaluation of fluvial to marginal marine sealing facies. *Marine and Petroleum Geology* **2009**, 26(4), 445-56, doi.org/10.1016/j.marpetgeo.2009.01.013.
74. Harding, A.; Strebelle, S.; Levy, M.; Thorne, J.; Xie, D.; Leigh, S.; Preece, R.; Scamman, R. Reservoir facies modelling: new advances in mps. *Geostatistics Banff 2004* **2005**, 559-568.
75. Pyrcz, M. J.; Strebelle, S.; Sun, T. Conditioning of object or event based reservoir models using local multiple-point statistics simulations. United States patent application No. 14/510,357, 2016.
76. Cojan, I.; Fouche, O.; Lopez, S. Process-based reservoir modeling in the example meandering channel. *Geostatistics Banff 2004* **2005**, 611-619.
77. Deutsch, C.V.; Wang, L. Hierarchical object-based stochastic modeling of fluvial reservoirs. *Mathematical Geology* **1996**, 28(7), 857-880.
78. Doyleand, J. D.; Sweet, M. L. Three-Dimensional Distribution of Lithofacies, Bounding Surfaces, Porosity, and Permeability in a Fluvial Sandstone—Gypsy Sandstone of Northern Oklahoma. *AAPG Bulletin* **1995**, 79(1), 70-95.
79. Hove, A.; Colombera, L.; O'Connor, V. S.; Cobain, S.; Mountney, N.; Meyer, B. A Novel Approach for Directly Informing Facies Modelling Algorithms with High Quality Ancient and Modern Analogue Databases, 79th EAGE Conference and Exhibition, 2017, doi.org/10.3997/2214-4609.201700609.
80. Ruiu, J.; Caumon, G.; Viseur, S. Modeling channel forms and related sedimentary objects using a boundary representation based on non-uniform rational B-splines. *Mathematical Geosciences* **2016**, 48(3), 259-284, doi.org/10.1007/s11004-015-9629-3.
81. Emerick, A. A. Investigation on Principal Component Analysis Parameterizations for History Matching Channelized Facies Models with Ensemble-Based Data Assimilation. *Mathematical Geosciences* **2017**, 49(1), 85-120, doi.org/10.1007/s11004-016-9659-5.

82. Cumella, S. P.; Ostby D. B. Geology of the basin-centered gas accumulation, Piceance Basin, Colorado. In *Piceance Basin 2003 Guidebook*, Peterson, K. M.; Olsen T. M.; Anderson D. S., Denver: Rocky Mountain Association of Geologists, 2003, pp. 171–93.
83. Trendell, A. M.; Atchley S. C.; Nordt, L. C. Facies analysis of a probable large-fluvial-fan depositional system: the Upper Triassic Chinle Formation at Petrified Forest National Park, Arizona, USA. *Journal of Sedimentary Research* **2013**, 83(10), 873-895, doi.org/10.2110/jsr.2013.55.
84. Lee, S. Y.; Carle, S. F.; Fogg, G. E. Geologic heterogeneity and a comparison of two geostatistical models: Sequential Gaussian and transition probability-based geostatistical simulation. *Advances in Water Resources* **2007**, 30(9), 1914-1932, doi.org/10.1016/j.advwatres.2007.03.005.
85. Gani, M. R.; Alam, M. M. Fluvial facies architecture in small-scale river systems in the Upper Dupi Tila Formation, northeast Bengal Basin, Bangladesh. *Journal of Asian Earth Science* **2004**, 24(2), 225-236, doi.org/10.1016/j.jseaes.2003.11.003.
86. Alam, M. M.; Curray, J. R.; Chowdhury, M. L.; Gani, M. R. An overview of the sedimentary geology of the Bengal Basin in relation to the regional tectonic framework and basin-fill history. *Sedimentary Geology* **2003**, 155(3), 179–208, doi.org/10.1016/S0037-0738(02)00180-X.
87. Goodbred, S. L.; Kuehl, S. A.; Steckler, M. S.; Sarker, M. Controls on facies distribution and stratigraphic preservation in the Ganges–Brahmaputra delta sequence. *Sedimentary Geology* **2003**, 155, 301–316, doi.org/10.1016/S0037-0738(02)00184-7.
88. Cheng, S.; Jiang, Y.; Li, J.; Li, C.; Wang, Y.; Xu, L. Reservoir prediction in a development area with a high-density well pattern using seismic sedimentology: An example from the BB2 block, Changyuan LMD oil field, Songliao Basin, China. *Interpretation* **2015**, 3(3), SS87-99, doi.org/10.1190/INT-2014-0229.1.
89. Dongmei, C.; Lanying, H.; Liying, Y.; Yajie, G.; Mian, L. Application of the seismic sedimentology in predicting narrow channel sand bodies. Beijing International Geophysical Conference & Exposition, Beijing, China, 2014, pp. 868-871, doi.org/10.1190/IGCBeijing2014-220.
90. Zhu, H.; Yang, X.; Zhou, X.; Liu, K. Three-dimensional facies architecture analysis using sequence stratigraphy and seismic sedimentology: Example from the Paleogene Dongying Formation in the BZ3-1 block of the Bozhong Sag, Bohai Bay Basin, China. *Marine and Petroleum Geology* **2014**, 51, 20-33, doi.org/10.1016/j.marpetgeo.2013.11.014.
91. Ross-Coss, D.; Ampomah, W; Cather, M; Balch, R. S.; Mozley, P.; Rasmussen, L. An improved approach for sandstone reservoir characterization. Western Regional Meeting, Society of Petroleum Engineers, USA, 2016, pp. 1-15, doi.org/10.2118/180375-MS.
92. Ambrose, W.A.; Loucks, R.G.; Dutton, S.P. Sequence-Stratigraphic and Depositional Controls on Reservoir Quality in Lowstand Incised-Valley Fill and Highstand Shallow-Marine Systems in the Upper Cretaceous (Cenomanian) Tuscaloosa Formation, Louisiana, USA. *GCAGS Journal* **2014**, 4, 43-66.
93. Ahokas, J. M.; Nystuen, J. P.; Martinius, A. W. Stratigraphic signatures of punctuated rise in relative sea-level in an estuary-dominated heterolithic succession: Incised valley fills of the Toarcian Ostreaelv Formation, Neill Klinter Group (Jameson Land, East Greenland). *Marine and Petroleum Geology* **2014**, 50, 103-129, doi.org/10.1016/j.marpetgeo.2013.11.001.
94. Rasmussen, E. S. Development of An Incised-Valley Fill Under the Influence of Tectonism and Glacio-Eustatic Sea-Level Change: Valley Morphology, Fluvial Style, and Lithology. *Journal of Sedimentary Research* **2014**, 84(4), 278-300, doi.org/10.2110/jsr.2014.24.
95. Flood, R. D.; Damuth, J. E. Quantitative characteristics of sinuous distributary channels on the Amazon deep-sea fan. *GSA Bulletin* ***1987***, 98(6),728-738, doi.org/10.1130/0016-7606(1987)98<728:QCOSDC>2.0.CO;2.